

Eosin Y derivatives for Visible Light-mediated Free-Radical Polymerization: Applications in 3D-Photoprinting and Bacterial Photodynamic Inactivation.

Lucie Pierau¹, Jean-Pierre Malval², Samir Abbad Andaloussi³, Annalisa Chiappone⁴, Sonia Lajnef⁵, Fabienne Peyrot^{5,6}, Steffen Jockusch⁷, Davy-Louis Versace^{1*}

¹University Paris-Est Creteil, CNRS, ICMPE, UMR 7182, 94320 Thiais, France

²Institut de Science des Matériaux de Mulhouse, UMR CNRS 7361, Université de Haute Alsace, 15 Rue Jean Starcky, 68057 Mulhouse, France

³Université Paris-Est Créteil (UPEC), Laboratoire Eau, Environnement, Systèmes Urbains (LEESU), UMR-MA 102, 61 avenue Général de Gaulle, 94010 Créteil Cedex, France

⁴Dipartimento di Scienze Chimiche e Geologiche, Università degli Studi di Cagliari, Via Università 40, 09124 Cagliari, Italy

⁵Laboratoire de Chimie et Biochimie Pharmacologiques et Toxicologiques, Université Paris Cité, 75006 Paris, France

⁶Institut National Supérieur du Professorat et de l'Éducation (INSPE) de l'Académie de Paris, Sorbonne Université, 10 rue Molitor, 75016 Paris, France

⁷Center for Photochemical Sciences, Bowling Green State University, Bowling Green, Ohio 43403, USA

Abstract

This study reports the design and subsequent use of mono-allylated (**EY-MA**) and di-allylated (**EY-DA**) derivatives of eosin Y (EY) as highly efficient visible light-sensitive photosensitizers (PS) of bio-based H-donor molecules (cysteamine (Cys) or *N*-acetyl-*L*-cysteine (NAC)) and an electron donor compound (*N*-methyldiethanolamine, MDEA) for free-radical and thiol-acrylate polymerizations of a bio-based monomer derived from soybean oil (SOA). High final acrylate conversions for SOA polymerization (up to 80%) evidence the efficient photoinitiating properties of the eosin derivatives systems under LEDs@405, 455 and 505 nm irradiation, and outperform those obtained with EY and other common photosensitizers such as camphorquinone or benzophenone. As described by fluorescence and phosphorescence analyses, laser flash photolysis (LFP) and electron paramagnetic resonance spin-trapping (EPR-ST) experiments, **EY-MA** and **EY-DA** can react via a proton/proton-coupled electron transfer reaction with Cys (or NAC) and MDEA respectively. The efficient singlet oxygen generation of the **EY-MA**-based materials upon exposure to visible light leads to tremendous antibacterial properties, against both Gram-positive *Staphylococcus aureus* (*S. aureus*) and Gram-negative *Escherichia coli* (*E. coli*). A 3-log decrease of *E. coli* adhesion on the surface of the materials is observed and 100% adhesion inhibition of *S. aureus* is also demonstrated. The co-polymerization of the eosin-derived PS with the polymer matrix ensures sustainable antibacterial properties against both bacteria strains upon visible light exposure as it prevents their leakage out of the polymer network.

Finally, finely complex 3D structures are successfully obtained by a 3D-photoprinting technology with the investigated **EY-MA**-based formulation using LED@405 nm.

Keywords: eosin Y, free-radical photopolymerization, visible light, antibacterial activity, 3D-photoprinting.

Introduction

UV light photo-initiating systems have been widely used in free-radical photopolymerization (FRP) due to their rapid curing and versatility. However, some severe limitations are associated to these systems such as the limitation of curing depth, significant shrinkage and stress within the cured materials or health and safety risks to operators including skin and eyes damage¹⁻⁴. Addressing these issues requires either a thorough understanding of the photopolymerization processes, the optimization of the processing parameters or the design of innovative visible-light absorbing photo-initiating systems (PISs). The emergence of visible-light PISs represents significant advances in the field of photopolymerization, offering exciting prospects for overcoming the limitations of traditional UV-light curing⁵. Ongoing research and innovation in this domain are on the course to revolutionize the development of novel materials, technologies, and applications across various fields, including coatings, adhesives, 3D printing, and biomedical materials⁶⁻⁸. Considering these factors, numerous efforts have been undertaken to design novel visible-light photosensitive systems, aiming to surmount the limitations of the aforementioned UV-light absorbing systems. Norrish I and II type PISs, which operate within the visible spectrum, are widely recognized for their ability to facilitate free-radical polymerization⁹⁻²³. Recent advances in FRP using visible light-sensitive PISs have been outlined in comprehensive reviews^{3,6,7}.

Surprisingly, PISs derived from eosin Y (EY) have been scarcely studied for FRP applications despite their intriguing light-absorbing characteristics. EY is a well-known synthetic dye belonging to the xanthene group, commonly used as a colouring agent for the food, cosmetics, pharmaceuticals and textile industries²⁴, for its photoreduction properties against nitrobenzene derivatives²⁵, as an analytical probe²⁶, in biological staining²⁷ and as a catalyst in photoredox organic reactions^{28,29}. EY particularly stands out as a remarkable organic photocatalyst, demonstrating noticeable utility in the formation of hydrogels under ambient conditions and low-intensity visible light irradiation, requiring sub-micromolar concentrations^{30,31}. The addition of tertiary amines to EY has been described as an efficient PIS for the FRP of several monomers in homogeneous media³²⁻³⁷. Furthermore, the EY/tertiary amine PISs are particularly interesting as FRP can occur despite the presence of an excess of several

radical polymerization inhibitors³¹. Notably, this PIS has been employed for surface modification by surface-mediated polymerization³⁸. Interestingly, EY appears among the most effective photoinitiator (PI) to initiate acrylamide photopolymerization compared with other xanthene dyes³⁹.

To date, the EY photopolymerization systems have found uses in radical polymerization within aqueous biological settings, employing low-intensity visible light irradiation. For instance, the two-component PIS based on EY and triethanolamine (TEA) has been activated by visible light to generate free radicals for the synthesis of new hydrogels by FRP. In order to accelerate the gelation kinetics, different co-monomers such as *N*-vinyl caprolactam (VC) or 1-vinyl-2-pyrrolidinone (NVP) are usually introduced to the crosslinking solution. To understand how the crosslinking conditions impact the properties of the resulting photo-induced hydrogel, Sharifi et al. conducted a comprehensive investigation wherein the concentrations of the crosslinking agents (EY, TEA, and VC) and the gelatin methacrylate monomer, and the irradiation time independently varied⁴⁰. Subsequently, they studied for each aforementioned parameter the ensuing modifications of the chemical, physical, mechanical, and biological attributes of the hydrogel. Importantly, EY and TEA, when combined and copolymerized with NVP, were often used as a visible light-sensitive system for the radical production and therefore the synthesis of various hydrogels based on acrylate, thiol–vinyl and thiol–ene monomer processes^{41,42}. EY has been also employed with TEA to initiate the bulk gelation of cell-laden tissue engineering scaffolds, resulting in high reported cell viability. In this investigation, Bahney et al. established non-toxic conditions for the photo-encapsulation and the viability enhancement of human mesenchymal stem cells (hMSCs) within poly(ethylene glycol) diacrylate hydrogel scaffolds using a EY/TEA/NVP-based PIS⁴³. Recently, Zhang et al. reported the use of a novel white light-sensitive PIS based on EY/*N*-phenylglycine (NPG) for the synthesis of a biocompatible and injectable composite hydrogel methacrylate alginate⁴⁴.

Several studies also reported the use of EY as a photosensitizer (PS) for bacterial photodynamic inactivation (PDI) thanks to its high singlet oxygen ($^1\text{O}_2$) yield. Efficient antibacterial activities were indeed reported for EY against a large panel of bacteria strains^{45–47}, including foodborne bacteria⁴⁸ and in dentistry⁴⁹. However, some studies also mentioned that deposited EY slowly leaked from their material support into the investigated medium^{17,50,51}. If this can be an attractive feature for applications such as drug delivery, it also limits its use as a sustainable antibacterial agent while raising environmental concerns in other application fields. To answer this constraint, covalently immobilizing EY to various supports has been studied for bacterial PDI applications, like for example a bioconjugate between EY and an antibacterial peptide with enhanced antimicrobial properties⁵² or an EY-based multifunctional polycation featuring primary and quaternary ammoniums as well as hydroxyl moieties for anti-infective therapy⁵³.

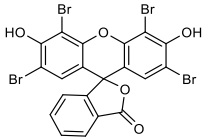
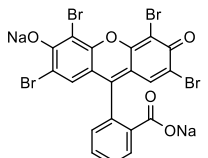
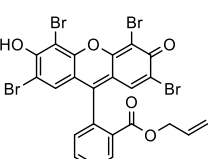
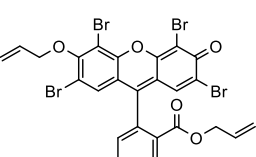
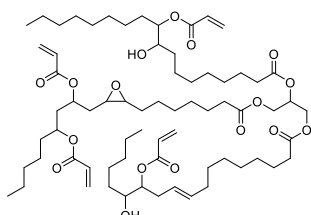
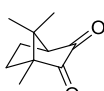
In this work, we combined the ability of EY to successfully initiate polymerization reactions upon exposure to a visible light source with its ability to efficiently generate reactive oxygen species (ROS) under irradiation. In the present investigation, EY is additionally used as a copolymerizable monomer since allyl moieties have been grafted on the EY structure via a simple one-step procedure. Two EY derivatives (**EY-MA** and **EY-DA**) are hence synthesized and characterized. Their photochemical behaviours are studied upon exposure to visible light sources, namely light emitting diodes (LED) working at 405, 455, 470, 505, 530 and 590 nm. Real-time Fourier Transform IR spectroscopy is used to investigate the performance of the EY derivatives to successfully initiate free radical and thiol-acrylate photopolymerization reactions in the presence of *N*-methyldiethanolamine (MDEA, an electron-donor), cysteamine (Cys) and *N*-acetyl-*L*-cysteine (NAC), H-donor thiol compounds. Steady-state photolysis, luminescence as well as electron paramagnetic resonance spin-trapping (EPR-ST) experiments are carried out to understand the initiation mechanisms involved under light irradiation. Polymer materials incorporating EY derivatives are then obtained and tested for efficient ROS generation under visible light exposure while release tests are performed to confirm the absence of leakage of the PIs over time. Photo-rheology analysis enables to study the mechanical properties of the photogenerated polymer materials and 3D-photoprinting experiments are carried out to demonstrate the potential of the PISs investigated here to be used in the design of complex 3D-structures. Finally, the antibacterial properties of the photoinduced materials are tested against *Staphylococcus aureus* (*S. aureus*) and *Escherichia coli* (*E. coli*) under irradiation with a solar emission lamp.

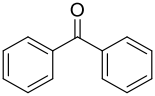
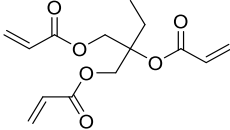
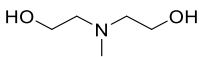
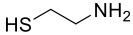
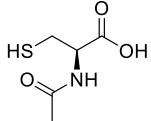
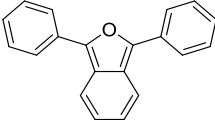
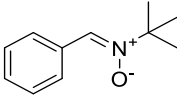
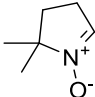
Experimental part

Materials. Eosin Y (EY, ~ 99%), allyl bromide (99%), tetraethylammonium bromide (TEAB, phase-transfer catalyst, 98%), hydrochloric acid (HCl, 37%), *N*-methyldiethanolamine (MDEA, > 99%), cysteamine (Cys, ~ 95%), soybean oil epoxidized acrylate (SOA), 5,5-dimethyl-1-pyrroline *N*-oxide (DMPO), *N*-tert-butyl- α -phenylnitron (PBN) and 1,3-diphenylisobenzofuran (DPBF, 97%) were provided by Sigma Aldrich. Acid red 87 (AR87, > 90%) was provided by TCI and tetraethylammonium tetrafluoroborate (NEt₄BF₄, 99%) was provided by Alfa Aesar. Potassium carbonate (K₂CO₃, > 99%) was provided by Labkem and *N*-acetyl-*L*-cysteine (NAC, 98%) was provided by Janssen. Trimethylolpropane triacrylate (TMPTA) was provided by Sartomer. Ethanol (EtOH), methanol (MeOH), dimethylformamide (DMF), acetonitrile (ACN), cyclohexane (CyH), dichloromethane (DCM), ethyl acetate (EtOAc), tetrahydrofuran (THF), silica gel and magnesium sulphate (MgSO₄) were obtained from commercial

suppliers. All reactants and solvents were used without further purification. Table 1 displays the chemical structures of the main compounds used in this study.

Table 1. Chemical structures of the compounds discussed in this study.

Name	Chemical structure	Role
Eosin Y (EY)		Photosensitizer (PS)
Acid red 87 (AR87)		PS
Eosin Y mono-allyl (EY-MA)		PS
Eosin Y di-allyl (EY-DA)		PS
Soybean oil epoxidized acrylate (SOA)		Acrylate monomer
Camphorquinone (CQ)		PS

Benzophenone (BP)		PS
Trimethylolpropane triacrylate (TMPTA)		Acrylate monomer
<i>N</i> -methyl-diethanolamine (MDEA)		Electron and H-donor co-initiator
Cysteamine (Cys)		H-donor co-initiator
<i>N</i> -acetyl-L-cysteine (NAC)		H-donor co-initiator
1,3-diphenylisobenzofuran (DPBF)		Singlet oxygen (¹ O ₂) trap
<i>N</i> -tert-butyl- α -phenylnitron (PBN)		Spin trap
5,5-dimethyl-1-pyrroline <i>N</i> -oxide (DMPO)		Spin trap

Methods.

Synthesis of allyl 2-(2,4,5,7-tetrabromo-6-hydroxy-3-oxo-3H-xanthen-9-yl)benzoate (EY-MA, Figure 1). A mixture of AR87 (1.00 g, 1.45 mmol) and allyl bromide (1.5 mL, 17 mmol) in DMF (6 mL) was stirred at 85 °C overnight. Upon completion, the reaction mixture was poured into 100 mL of an aqueous solution of HCl under continuous stirring ([HCl] = 0.1 M). The solution was then filtered to afford a red crude solid. The crude product was purified by column chromatography (SiO₂, ethyl acetate-methanol 9:1) to give **EY-MA** as a shiny dark red powder in 44-53% yield.

¹H NMR (400 MHz, methanol-d₄, **Error! Reference source not found.**-A), δ (ppm): 8.27 (d, J = 7.3 Hz, 1H, H19), 7.86 (t, J = 7.1 Hz, 1H, H17), 7.80 (t, J = 7.6 Hz, 1H, H18), 7.48 (d, J = 7.4 Hz, 1H, H16), 7.17

(s, 2H, H3 & H11), 5.60 – 5.48 (m, 1H, H31), 5.09 – 5.00 (m, 2H, H32), 4.44 (d, J = 5.9 Hz, 2H, H30). ¹³C NMR (101 MHz, methanol-*d*₄, **Error! Reference source not found.-A** and **Error! Reference source not found.-A**), δ (ppm): 171.66 (C1 & C13), 166.48 (C21), 155.25 (C5 & C9), 155.12 (C7), 134.83 (C15), 133.96 (C17), 132.38 (C31), 132.14 (C19), 131.99 (C20), 131.76 (C16), 131.43 (C18), 131.20 (C3 & C11), 120.03 (C4 & C8), 119.66 (C32), 113.12 (C2 & C12), 101.25 (C6 & C14), 67.07 (C30). IR (neat, cm⁻¹, **Error! Reference source not found.**): 2957 (ν_{CH2}), 2924 (ν_{CH}), 2858 (ν_{CH2}), 1714 (ν_{C=O}), 1618 (ν_{C=C}), 1551 (ν_{C=C}), 1501 (δ_{CH2}), 1454 (ν_{C=C}), 1346 (δ_{OH}), 1260 (ν_{CO-OC}), 1234 (ν_{C-OH}), 1171 (δ_{CH}), 1128 (ν_{CO-OC}), 1078 (δ_{CH}), 1057 (δ_{CH}), 974 (γ_{CH}), 877 (γ_{CH2}), 760 (γ_{CH}), 710 (γ_{CH}), 640, 573, 469, 444 (skeletal vibrations). LC-MS (**Error! Reference source not found.**): m/z [ESI⁺]: expected (C₂₃H₁₂Br₄O₅) 687.96, found 687.84.

Synthesis of allyl 2-(6-(allyloxy)-2,4,5,7-tetrabromo-3-oxo-3H-xanthen-9-yl)benzoate (EY-DA, Figure 1). A mixture of K₂CO₃ (0.34 g, 2.47 mmol) and tetraethylammonium bromide (TEAB, 13.0 mg, 0.06 mmol) was powdered in a mortar and added to EY (0.20 g, 0.31 mmol) into a 30 mL microwave tube equipped with a magnetic stirrer and a cap. Allyl bromide (5 mL, 58 mmol) was added to the mixture and the heterogeneous solution was let to react under pressure at 85 °C for 90 min under microwave irradiation. Upon completion, the reaction mixture was poured into 100 mL of distilled water. The solution was then extracted with 3 x 30 mL of DCM. The organic layer was dried with MgSO₄, filtered and the solvent was evaporated under reduced pressure to afford a red crude solid. The crude product was purified by column chromatography (SiO₂, dichloromethane-cyclohexane 7:3) to give **EY-DA** as an orange powder in 38% yield.

¹H NMR (400 MHz, CDCl₃, **Error! Reference source not found.-B**), δ (ppm): 8.36 (d, J = 7.5 Hz, 1H, H19), 7.83 (t, J = 7.4 Hz, 1H, H17), 7.78 (t, J = 7.5 Hz, 1H, H18), 7.34 (d, J = 7.4 Hz, 1H, H16), 7.28 (s, 1H, H11), 7.12 (s, 1H, H3), 6.26 – 6.13 (m, 1H, H31), 5.79 – 5.66 (m, 1H, H34), 5.49 (d, J = 17.1 Hz, 1H, H32a), 5.36 (d, J = 10.3 Hz, 1H, H32b), 5.26 – 5.15 (m, 2H, H35), 4.68 (d, J = 5.9 Hz, 2H, H30), 4.55 (d, J = 5.8 Hz, 2H, H33). ¹³C NMR (101 MHz, CDCl₃, **Error! Reference source not found.-B** and **Error! Reference source not found.-B**), δ (ppm): 172.42 (C1 & C13), 164.53 (C27), 157.64 (C5), 154.36 (C9), 149.45 (C7), 148.73 (C15), 133.55 (C17), 133.09 (C20), 132.22 (C31), 131.92 (C19), 131.01 (C18), 130.88 (C34), 130.59 (C16), 130.50 (C11), 130.16 (C12), 130.05 (C3), 127.49 (C8), 120.00 (C32), 119.89 (C4), 119.76 (C35), 114.88 (C2), 108.72 (C6), 102.63 (C14), 75.15 (C30), 66.42 (C33). IR (neat, cm⁻¹, **Error! Reference source not found.**): 1715 (ν_{C=O}), 1609 (ν_{C=C}), 1570 (ν_{C=C}), 1535 (ν_{C=C}), 1508 (ν_{C=C}), 1383 (δ_{CH2}), 1323 (δ_{CH}), 1263 (ν_{C-O-C}), 1186 (δ_{CH}), 1142 (ν_{C-O-C}), 1082 (δ_{CH}), 982 (γ_{CH}), 935 (γ_{CH2}), 760 (γ_{CH}), 706 (γ_{CH}), 656, 627, 565, 488, 419 (skeletal vibrations). LC-MS (**Error! Reference source not found.**): m/z [ESI⁺]: expected (C₂₆H₁₆Br₄O₅) 728.03, found 727.86.

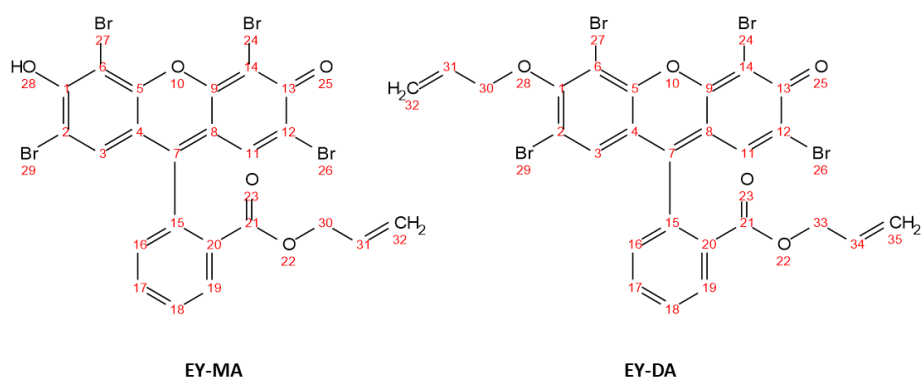


Figure 1. Chemical structures of EY-MA and EY-DA.

NMR, IR and LC-MS characterization. NMR spectra were measured on a Bruker Avance II instrument, with frequencies of 400 MHz and 101 MHz for ^1H and ^{13}C NMR respectively. IR spectra were collected on a PerkinElmer FT-IR spectrometer between 400 and 4000 cm^{-1} . LC-MS analyses were carried out by direct introduction on a HPLC Ultimate 3000 (Dionex) combined with a simple quadrupole mass spectrometer (Surveyor MSQ+, ThermoScientific, Massachusetts, USA) equipped with an electrospray source. Analytes were detected either in negative (ESI $^-$) or positive (ESI $^+$) ion mode. The pressure of the nebulizing gas N_2 applied to the device was 5.5 bar, source temperature 400 $^\circ\text{C}$, cone potential 75 V. The mobile phase was composed of ACN/water 7:3 with 0.1% formic acid addition. The flow rate was 0.2 mL per minute at 30 $^\circ\text{C}$ and volume injected was 2 μL .

UV-visible absorption spectra were recorded on an Agilent Technologies Cary 60 UV-Vis spectrophotometer in the 200-800 nm wavelength range, using 1 cm-wide quartz cuvettes at room temperature. ϵ values reported in ACN are mean values obtained from duplicates.

Irradiation sources. Visible Light Emitting Diodes (LEDs) irradiating at 405 nm (166 mW/cm^2), 455 nm (70 mW/cm^2), 470 nm (51 mW/cm^2), 505 nm (26 mW/cm^2), 530 nm (48 mW/cm^2) and 590 nm (79 mW/cm^2) were provided by THORLABS.

Steady-state photolysis experiments of AR87, **EY-MA** and **EY-DA** were conducted in acetonitrile under inert atmosphere, upon exposure to LED@405 nm (166 mW/cm^2). Their absorption spectra were recorded at fixed times and the photosensitizers were irradiated alone or in presence of MDEA, NAC or Cys. For solubility issues, the photolysis experiments carried out in presence of Cys were conducted in ethanol. In acetonitrile, concentrations used were $[\text{AR87}] = 8.7 \times 10^{-6}$ M, $[\text{EY-MA}] = 9.7 \times$

10^{-6} M and [EY-DA] = 5.6×10^{-5} M. In ethanol, the concentrations were [AR87] = 1.2×10^{-5} M, [EY-MA] = 1.2×10^{-5} M and [EY-DA] = 8.7×10^{-5} M. All the solutions were saturated with argon prior to the experiments.

Luminescence measurements. Steady-state fluorescence spectra were recorded on a Fluorolog-3P (HORIBA Jobin Yvon) spectrofluorometer and corrected for lamp intensity and detector response. Fluorescence lifetime measurements were performed by time-correlated single photon counting using an OB920 spectrometer (Edinburgh Analytical Instruments) in conjunction with a pulsed LED (456 nm or 495 nm, PicoQuant). For phosphorescence measurements, the sample solutions in ethanol were frozen in a quartz liquid nitrogen dewar (77 K). Time-resolved phosphorescence spectra were recorded on a Fluorolog-3P (HORIBA Jobin Yvon) spectrofluorometer using a pulsed Xe-lamp for excitation. Phosphorescence lifetime measurements were performed by multi-channel scaling using an OB920 spectrometer (Edinburgh Analytical Instruments) in conjunction with a pulsed Xe-lamp.

EPR experiments of EY-MA and EY-DA were carried out using an Elexsys E500 EPR spectrometer (Bruker, Wissembourg, France), operating at X-band (9.8 GHz) and equipped with an SHQ high-sensitivity cavity. Solutions composed of PI alone, PI/spin trap, PI/spin trap/co-initiator or spin trap/co-initiator (PI = EY-MA or EY-DA; co-initiator = MDEA, NAC or Cys; spin trap = DMPO or PBN) were prepared in a 4-mm quartz EPR tube at room temperature in either dry THF for EY-MA or in dry DCM for EY-DA. The solutions were purged for a minute with argon. The tube was sealed with a septum cap and irradiated either directly in or outside the EPR resonator using LED@405 nm (166 mW/cm^2). X-band EPR spectra were recorded before, during and after irradiation. Typical settings used were: microwave power, 10 mW; modulation frequency, 100 kHz; modulation amplitude, 0.05 mT; receiver gain, 60 dB; time constant, 10.24 ms; conversion time, 40.96 ms; datapoints, 1024; sweep width, 7 mT; sweep time, 41.94 s. Multiple EPR spectra for each sample were recorded sequentially at 21°C. The different figures present the sum of at least 5 experimental spectra. Data acquisition and processing were performed using Bruker Xepr software. The simulated spectra were calculated with the EasySpin toolbox working on MatLab platform⁵⁴.

Cyclic voltammetry. Cyclic voltammetry measurements of EY-MA and EY-DA were carried out using an AUTOLAB potentiometer/galvanometer in a standard three-electrode cell configuration. A vitreous carbon electrode, a gold wire and a saturated calomel electrode were used as working, counter and reference electrodes respectively. A solution of tetraethylammonium tetrafluoroborate ([NEt₄BF₄] = 10^{-3} M) in DMF was used as the supporting electrolyte. EY-MA and EY-DA were introduced at a concentration of 9×10^{-4} and 10^{-3} M respectively, and the electrochemical cell was placed under inert conditions thanks to an argon flow prior to measurement. Measurements were recorded with a

0.1 V.s⁻¹ scan rate and 0.025 V of step potential between 0 and 2.5 V for oxidation, and between 0 and -2.5 V for reduction. GPES electrochemical software 4.9 (Utrecht, Netherlands) was used to analyse data. The free energy change, ΔG_{eT} , for an electron transfer between **EY-MA** (EY or **EY-DA**) and a given co-initiator can be calculated from the classical Rehm-Weller equation⁵⁵ here after:

$$\Delta G_{eT} = E_{ox}(D) - E_{red}(A) - E^* + C \quad (1)$$

$E_{ox}(D)$ represents the electron donor oxidation potential, $E_{red}(A)$ represents the electron acceptor reduction potential, E^* represents the excited state spectroscopic energy and C is an electrostatic correction term.

Laser flash photolysis. Laser flash photolysis experiments employed the pulses from a Spectra Physics GCR-150-30 Nd:YAG laser (355 nm or 532 nm, ~7 ns pulse width) and a computer-controlled system, as described previously²⁶. Solutions of the eosin derivatives were prepared at concentrations such that the absorbance was ~ 0.3 in 1 × 1 cm quartz cells at the excitation wavelength (355 nm or 532 nm) for recording transient absorption spectra and quenching studies.

Photopolymerization kinetic studies. Photosensitive formulations were laid down on a BaF₂ pellet and irradiated at room temperature under air or in laminated conditions with different visible light sources. The laminated conditions were obtained by covering the formulation with a transparent polypropylene film. No previous degassing was carried out for sample preparation. The thickness of the samples was controlled by using optical density measurements. The BaF₂ pellets ($\varnothing 25 \pm 0.2$ mm × 5 ± 0.1 mm) were provided by Korth Kristalle GMBH. The polymerizations of each sample were recorded by real-time Fourier Transform InfraRed spectroscopy (RT-FTIR) on a JASCO FTIR 4700 Instrument. Real-time spectra were acquired in absorbance mode between 400 and 4000 cm⁻¹ with a resolution of 4 cm⁻¹. The decrease of acrylate group absorption band was followed at 1636 cm⁻¹ for SOA and TMPTA. Total conversion rates were calculated according to the following equation:

$$\text{Acrylate conversion (\%)} = \frac{A_0 - A_t}{A_0}$$

A_0 represents the acrylate peak surface area at $t = 0$ second and A_t represents the acrylate peak surface area at any time t .

Pellets synthesis. Formulations composed of AR87/MDEA/SOA, **EY-MA**/MDEA/SOA, **EY-DA**/MDEA/SOA or **EY-MA**/NAC/SOA (with 0.5 wt% of PI and 2 wt% of co-initiators with respect to the monomer) were laid in silicone moulds with a 15 mm diameter. They were irradiated in laminated conditions for 10 min on each side with a LED@405nm (166 mW/cm²). The pellets thus synthesized were then softly washed with EtOH. 13 mm-wide and tack-free materials were obtained.

Release experiments. Pellets obtained from the PI/MDEA/SOA formulations (PI = AR87, **EY-MA** or **EY-DA**) were immersed in 10 mL of acetonitrile. Samples were continuously agitated on an orbital shaker, and the solutions were sampled at fixed times to follow the release kinetics of the different PS by UV-visible spectroscopy. The percentages of AR87, **EY-MA** and **EY-DA** released from the pellets were determined applying Beer-Lambert's law at 529 nm ($\epsilon = 110,000 \text{ L}\cdot\text{mol}^{-1}\cdot\text{cm}^{-1}$), 538 nm ($\epsilon = 97,000 \text{ L}\cdot\text{mol}^{-1}\cdot\text{cm}^{-1}$) and 472 nm ($\epsilon = 17,000 \text{ L}\cdot\text{mol}^{-1}\cdot\text{cm}^{-1}$) respectively.

Singlet oxygen detection. The $^1\text{O}_2$ photogeneration by **EY-MA** was investigated in solution using DBPF as a common $^1\text{O}_2$ trap. The progress of $^1\text{O}_2$ generation was followed by the oxidation of DPBF, hence by the subsequent decrease of its absorbance at 410 nm. A solution containing both DPBF and **EY-MA** was prepared in methanol ($1.5 \times 10^{-5} \text{ M}$ and $3.9 \times 10^{-6} \text{ M}$ for DPBF and for **EY-MA** respectively). The solution was irradiated with a LED@530nm ($13.3 \text{ mW}/\text{cm}^2$) and sampled at fixed times to monitor the decrease of DPBF absorption by UV-visible spectroscopy. The reference test was carried out by irradiating a solution of DPBF in the absence of **EY-MA**, to account for its own photobleaching in the conditions used during the analysis.

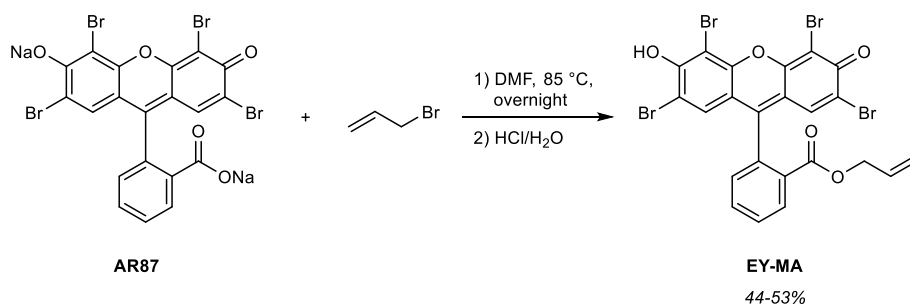
Antibacterial experiments. The antibacterial performance of the **EY-MA**/NAC/SOA-based material was assessed against strains of *S. aureus* (ATCC6538) and *E. coli* (ATCC25922). Pellets obtained with the **EY-MA**/NAC/SOA formulation were immersed in bacteria solutions ($10^6 \text{ CFU}/\text{mL}$) the night before the experiment to maximize bacteria adhesion on their surface. Half of these pellets were then exposed to a solar emission lamp for 1 hour on each side while the other half was kept in the dark. Following incubation and adhesion, the samples were rinsed seven times with sterilized saline solution (NaCl, 9 g/L) to wash any non-adherent cell off. The pellets were then transferred to 3 mL of sterilized saline solution and sonicated for 5 minutes to collect adherent bacteria. The bacterial suspensions were serially diluted 5 times and 100 μL each diluted solution were introduced onto petri dishes and plated with warm PCA. Colony forming units (CFUs) were counted after 48 hours of static incubation at 37 °C. The data reported herein are average results of triplicate experiments.

Real-time photorheology tests. They were performed using an Anton Paar MCR 302 compact rheometer to mimic the VAT photopolymerization DLP printing process. The instrument was equipped with a quartz bottom plate and a light source (LED@405nm, $40 \text{ mW}/\text{cm}^2$) was placed under the bottom plate. **EY-MA**/MDEA/SOA and **EY-MA**/NAC/SOA formulations were tested ([**EY-MA**] = 0.5 wt%; [MDEA] = [NAC] = 2 wt%). Measurements were performed at 25 °C. The gap between the two plates was set to 0.1 mm. The sample was kept under a constant shear frequency of 1 Hz and constant amplitude of 1% (LVE region, according to preliminary amplitude sweep measurements). Light was switched on after 60 s to allow the system to stabilize before the onset of polymerization.

3D-printing experiments. The 3D photosensitive formulations (**EY-MA**/MDEA/SOA and **EY-MA**/NAC/SOA with [**EY-MA**] = 0.5 wt% and [MDEA] = [NAC] = 2 wt%) were printed using a Asiga PICO 2 DLP printer with nominal XY resolution of 50 μm , using a diode as light-emitting source (405 nm, 40 mW/cm^2). The printing tests were performed keeping the vat at a constant temperature of 50°C to decrease the viscosity and facilitate the process. Printing parameters were experimentally set as follows: a) layer thickness of 50 μm and b) layer exposure time of 8 s for samples using MDEA as co-initiator and 40 s for samples using NAC. A post curing process was performed during 5 min with a medium-pressure mercury lamp (12 mW/cm^2 , Robot Factory).

Results and discussion

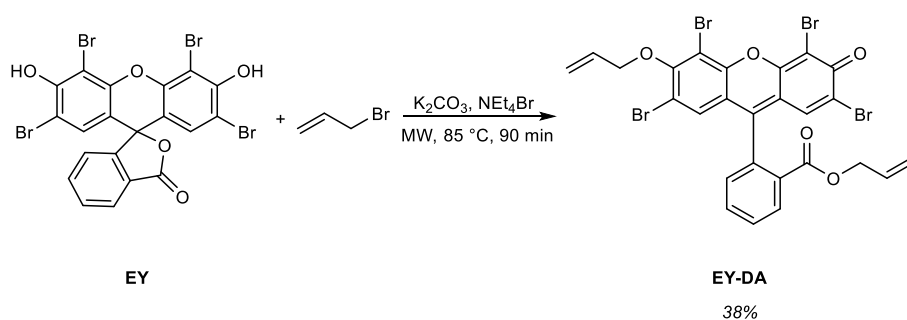
Synthesis and absorption properties of eosin-Y derivatives. Mono-allylated eosin Y (**EY-MA**) and di-allylated eosin Y (**EY-DA**) were synthesized following a one-step procedure each. Their respective reaction pathways are summarized in Scheme 1 and Scheme 2. The eosin Y derivatives obtained were characterized by ^1H , ^{13}C , DEPT 135, HSQC, HMBC and COSY NMR (Error! Reference source not found., Error! Reference source not found.), FTIR (Error! Reference source not found. and Error! Reference source not found.) and LC-MS (Error! Reference source not found. and Error! Reference source not found.).



Scheme 1. General procedure for the synthesis of **EY-MA**.

The mono-allylation of EY was inspired by a procedure previously reported in the literature⁵⁷. The reaction was carried out in DMF using allyl bromide and eosin Y disodium salt (**AR87**). The reaction was stirred at 85 °C overnight and its purification by column chromatography on silica gel afforded **EY-MA**

in an average yield ranging from 44% to 53%. ¹H NMR analysis confirmed the effective mono-allylation of EY with the appearance of allylic hydrogen signals at 4.45 ppm (d, 2H), 5.05 ppm (m, 2H) and 5.54 ppm (m, 1H) (**Error! Reference source not found.-A**). 2D NMR data also indicated the selective formation of the allyl ester derivative rather than the allyl phenyl ether isomer, as shown by the correlation peak between H30 and C21 on the HMBC NMR spectrum (**Error! Reference source not found.-A**). Previous studies dealing with the functionalization of various fluorescein derivatives such as erythrosin^{58,59}, rose bengal and eosin Y^{35,60–63} also reported that alkylation happened preferably on the available carboxylate function rather than the phenoxide group.



Scheme 2. General procedure for the synthesis of **EY-DA**.

The double allylation of EY is inspired by a previously described procedure carried out in a sealed vial under microwave irradiation^{14,17}. Allyl bromide was used as a solvent for the mixture of EY and NEt₄Br. The reaction was stopped after 90 minutes at 85 °C. The purification via column chromatography on silica gel gave the di-allylated derivative (**EY-DA**) with a 38% yield. ¹H NMR analysis confirmed the presence of two new allyl groups on the EY structure. The appearance of new hydrogen signals at 4.55 ppm (d, 2H), 4.68 ppm (d, 2H), 5.21 ppm (dd, 2H), 5.36 ppm (d, 1H), 5.46 ppm (d, 1H), 5.71 ppm (m, 1H) and 6.20 ppm (m, 1H) are assigned to the allyl groups of **EY-DA** (**Error! Reference source not found.-B**)⁶⁴.

Normalized absorption spectra of the different derivatives in acetonitrile are superimposed in Figure 2. The carboxylate alkylation of EY has a negligible impact on its absorption properties, as showcased by Figure 2, since phenol ionization remains possible to retain xanthene colour^{61,65,66}. Results show indeed similar absorption maxima between AR87, the fully ionized form of EY ($\lambda = 529$

nm, $\epsilon = 110,000 \text{ L}\cdot\text{mol}^{-1}\cdot\text{cm}^{-1}$), and **EY-MA** ($\lambda = 538 \text{ nm}$, $\epsilon = 97,000 \text{ L}\cdot\text{mol}^{-1}\cdot\text{cm}^{-1}$), with only a 9 nm-red-shift in λ_{max} for **EY-MA**, due to an increased electron donation through the ester function⁵⁹.

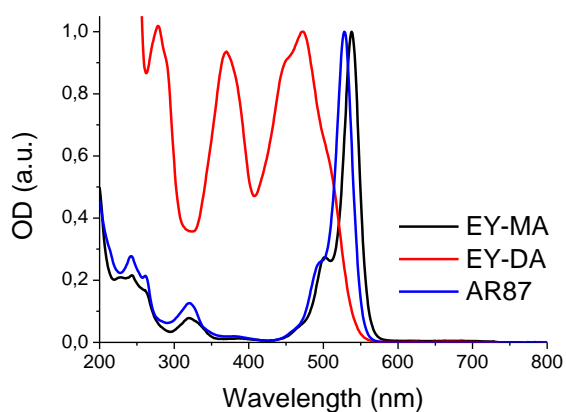


Figure 2. Normalized UV-visible spectra of AR87, **EY-MA** and **EY-DA** in acetonitrile.

On the contrary, the structural modification of the chromophoric part of EY causes an important blue-shift of the absorption spectrum. **EY-DA** presents two absorption maxima at $\lambda = 370 \text{ nm}$ and $\lambda = 472 \text{ nm}$ ($\epsilon_{472\text{nm}} = 17,000 \text{ L}\cdot\text{mol}^{-1}\cdot\text{cm}^{-1}$) in acetonitrile. Phenol functionalization prevents it from ionizing, which strongly influences its absorption properties towards the blue region^{61,66}. The derivatives obtained in this work still feature high absorptions up to 540 nm in the visible light range with high molar absorption coefficients, making them relevant candidates for their use as visible-light photosensitizers.

Photochemical reactivity of EY derivatives. The reactivities of AR87, **EY-MA** and **EY-DA** under visible-light irradiation were qualitatively evaluated by steady-state photolysis under inert atmosphere. Solutions of AR87 (**Error! Reference source not found.**), **EY-MA** (Figure 3) and **EY-DA** (Figure 4) in ACN or in EtOH were irradiated with LED@405 nm in presence or absence of either MDEA, Cys and NAC.

The photolysis experiments conducted on AR87 demonstrated a good stability when irradiated alone or mixed with MDEA. On the other hand, a gradual photobleaching of AR87 was observed when mixed with NAC or Cys upon exposure to blue light.

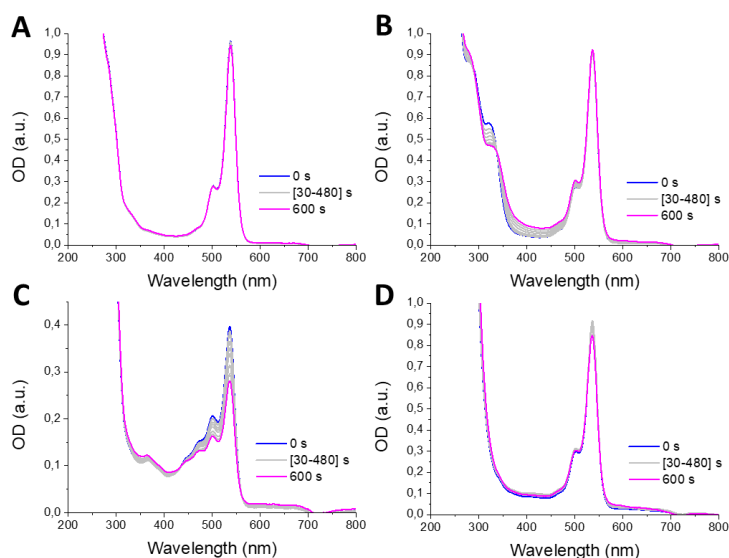


Figure 3. Steady-state photolysis of (A) **EY-MA**, (B) **EY-MA**/MDEA and (C) **EY-MA**/NAC in ACN, and of (D) **EY-MA**/Cys in EtOH under inert atmosphere, upon exposure to LED@405 nm. $[\text{EY-MA}] = 9.7 \times 10^{-6}$ M in ACN, $[\text{EY-MA}] = 1.2 \times 10^{-5}$ M in EtOH. $[\text{MDEA}] = 4.9 \times 10^{-2}$ M, $[\text{NAC}] = 4.9 \times 10^{-2}$ M and $[\text{Cys}] = 8.2 \times 10^{-2}$ M.

The photolysis experiments conducted on **EY-MA** showed a similar behaviour to AR87. The study highlights its relatively high photostability since no photobleaching was evidenced for the mono-functionalized derivative alone and when mixed with MDEA (Figure 3-A and Figure 3-B respectively). Although **EY-MA** underwent a slow photobleaching when mixed with Cys (Figure 3-D), the UV-vis changes are not significant enough to indicate a synergistic interaction between the PS and the considered co-initiator. The same trend was observed upon addition of NAC.

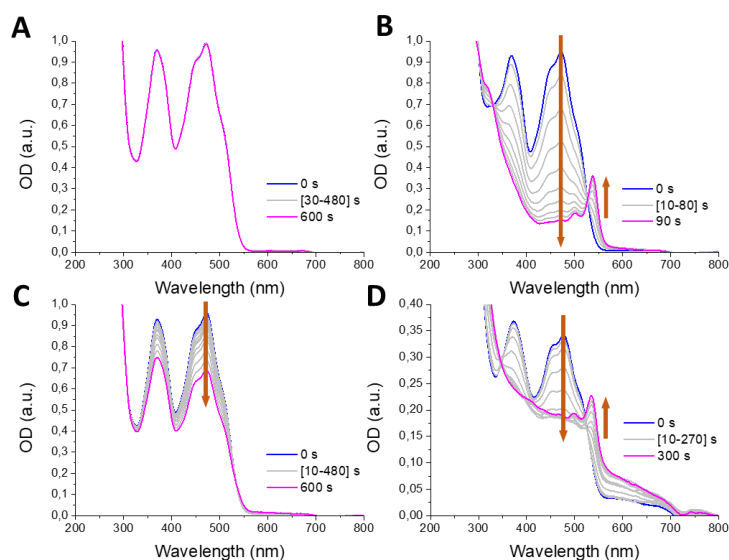


Figure 4. Steady-state photolysis of (A) **EY-DA**, (B) **EY-DA/MDEA** and (C) **EY-DA/NAC** in ACN, and of (D) **EY-DA/Cys** in EtOH under inert atmosphere, upon exposure to LED@405 nm. [**EY-DA**] = 5.6×10^{-5} M in ACN, [**EY-DA**] = 8.7×10^{-5} M in EtOH. [**MDEA**] = 4.9×10^{-2} M, [**NAC**] = 4.8×10^{-2} M and [**Cys**] = 2.6×10^{-2} M.

EY-DA demonstrated a good photostability when irradiated alone as well (Figure 4-A) while the addition of a co-initiator strongly decreased the absorption signal for all the co-initiators tested under irradiation. Fast photobleaching was indeed observed when **EY-DA** was mixed with MDEA (Figure 4-B), with Cys (Figure 4-D), as well as upon addition of NAC (Figure 4-C), though to a lesser extent in this case. These behaviours could indicate effective interactions occurring between the PS and the considered co-initiators. The photolysis experiments conducted on **EY-DA/MDEA** as well as on **EY-DA/Cys** also evidenced a new absorption band at 538 nm increasing under irradiation. This new band is associated to the cleavage of the phenyl ether bond in basic conditions and consequently to the formation of the related mono-functionalized derivative **EY-MA**, as indicated by the spectrum shape, the maximum absorption wavelength at 538 nm as well as the change in solution colour from orange to pink.

Excited state properties and quenching kinetics. To investigate the singlet excited state properties of the derivatives, fluorescence and cyclic voltammetry experiments were performed. The fluorescence emission spectrum of **EY-MA** (Figure 5-D, red line) is, as expected, similar to AR87, the fully ionized form of EY and shows a fluorescence lifetime of 4.4 ns. Also, **EY-DA** shows fluorescence (Figure 5-B, red line) with a lifetime of 0.96 ns. The fluorescence excitation spectra for both **EY-MA** and **EY-DA** (Figure 5-B,D, blue lines) match well with the absorption spectra (Figure 5-A,C), confirming that the observed fluorescence originates from **EY-MA** and **EY-DA**, respectively. The excited singlet state energies were determined from the wavelength where the excitation spectra intersect the emission spectra and are listed in Table 2.

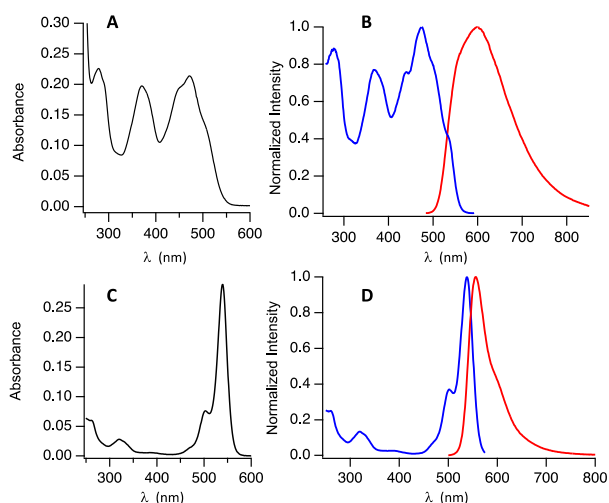


Figure 5. UV-vis absorption spectra of (A) **EY-DA** and (C) **EY-MA** in ACN. Fluorescence excitation (blue, $\lambda_{em} = 600$ nm) and emission (red, $\lambda_{ex} = 475$ nm) spectra of (B) **EY-DA** and (D) **EY-MA** in ACN.

The singlet excited state reactivity of the eosin derivatives with co-initiators were investigated by fluorescence quenching. **EY-MA** has a fluorescence lifetime of 4.4 ns. Upon addition of MDEA the fluorescence lifetime decreases. The bimolecular rate constant for the reaction of singlet excited states with MDEA was determined from the slope of the plot of the inverse fluorescence lifetime of **EY-MA** vs. the concentration of MDEA (Figure 6, left). The high rate constant ($k_q^{MDEA} = 5.0 \times 10^9 \text{ M}^{-1} \cdot \text{s}^{-1}$) ensures efficient initiator radical generation for polymerization. Rehm-Weller equation (see equation (1) in Methods) was used to determine if an electron transfer reaction was thermodynamically favourable

from MDEA to the singlet excited states of **EY-MA** and **EY-DA**. Using the reduction potentials of the functional PS, $E_{\text{red}}^{\text{EY-MA}} = -0.98 \text{ V/SCE}$ and $E_{\text{red}}^{\text{EY-DA}} = -0.85 \text{ V/SCE}$ (measured by cyclic voltammetry, **Error! Reference source not found.** and **Error! Reference source not found.**), the oxidation potential of MDEA, $E_{\text{ox}}^{\text{MDEA}} = 0.72 \text{ V/SCE}$ ⁶⁷, and the singlet excited state energies of the PS, $E_5^{\text{EY-MA}} = 2.27 \text{ eV}$ and $E_5^{\text{EY-DA}} = 2.33 \text{ eV}$ (extracted from the interception of their absorption and fluorescence emission spectra, Figure 5), negative values of free energy change were found in both cases ($\Delta G_{\text{et}}^{\text{EY-MA/MDEA}} = -0.57 \text{ eV}$ and $\Delta G_{\text{et}}^{\text{EY-DA/MDEA}} = -0.76 \text{ eV}$). This indicates that an electron transfer reaction is allowed. The rate constants for reaction of singlet excited states for **EY-MA** and **EY-DA** for other co-initiators were determined analogously (Figure 6 and Figure 7, respectively).

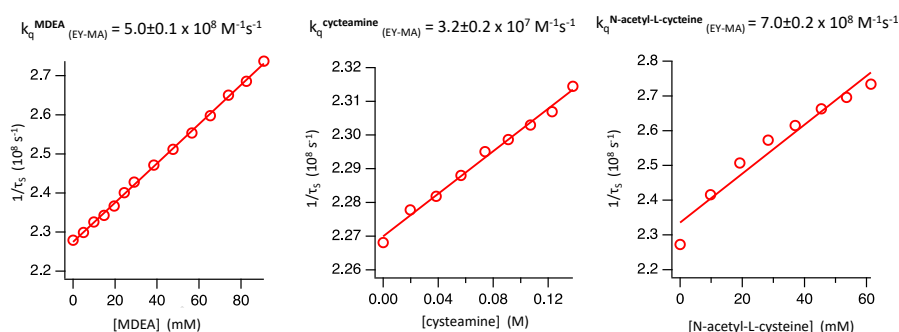


Figure 6. Determination of the bimolecular quenching rate constants k_q of **EY-MA** singlet states by MDEA (left), Cys (middle) and NAC (right) using fluorescence lifetime measurements ($\lambda_{\text{ex}} = 495 \text{ nm}$, pulsed LED). Inverse fluorescence lifetime of **EY-MA** ($\lambda_{\text{em}} = 562 \text{ nm}$) determined by time-correlated single photon counting vs. concentration of MDEA, Cys and NAC in ACN.

To investigate the triplet state reactivity of **EY-MA** and **EY-DA**, laser flash photolysis experiments were performed. Photoexcitation of **EY-MA** with laser pulses of 532 nm generated a transient absorption spectrum (Figure 8-A). The transient spectrum is dominated by ground state bleaching (negative signal) of **EY-MA** at 540 nm and shows a small positive signal at 590 nm which is assigned to the triplet state. The triplet state decayed with a lifetime of 56 μs (Figure 8-B) under recovery of the ground state absorption (Figure 8-C). Pulsed laser excitation (355 nm) of **EY-DA** generated a complex transient absorption spectrum with overlapping ground state and triplet state absorption (Figure 9-A). The isolated triplet state absorption was observable at $\sim 560 \text{ nm}$ which decayed with a lifetime of 23 μs under recovery of the ground state absorption (Figure 9-B to E).

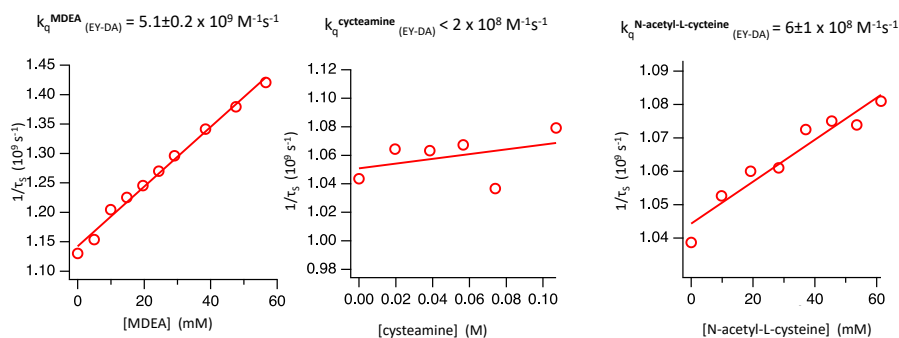


Figure 7. Determination of the bimolecular quenching rate constants k_q of **EY-DA** singlet states by MDEA (left), Cys (middle) and NAC (right) using fluorescence lifetime measurements ($\lambda_{\text{ex}} = 456 \text{ nm}$, pulsed LED). Inverse fluorescence lifetime of **EY-DA** ($\lambda_{\text{em}} = 600 \text{ nm}$) determined by time-correlated single photon counting vs. concentration of MDEA, Cys and NAC in ACN.

The triplet states of **EY-MA** and **EY-DA** were quenched by molecular oxygen with rate constants of $k_q^{\text{O}_2} = 2.1 \times 10^9 \text{ M}^{-1} \text{ s}^{-1}$ and $k_q^{\text{O}_2} = 1.4 \times 10^9 \text{ M}^{-1} \text{ s}^{-1}$, respectively (**Error! Reference source not found.**) which are typical for triplet states of organic molecules. The rate constants for reaction of the triplet state of **EY-DA** with the co-initiators MDEA and Cys were determined from the slope of the plot of the inverse triplet lifetime vs. the co-initiator concentration ($k_q^{\text{MDEA}} = 1.5 \times 10^8 \text{ M}^{-1} \text{ s}^{-1}$ and $k_q^{\text{Cys}} = 5.8 \times 10^6 \text{ M}^{-1} \text{ s}^{-1}$; **Error! Reference source not found.**). The rate constants for reactions from the triplet state are smaller than from the singlet excited state which is expected due to the lower energy of the triplet state compared to the singlet excited state (Table 2). However, the longer lifetime of the triplet state (23 μs) compared to the singlet excited state (0.96 ns) compensates for the lower rate constants. The reduction of **EY-DA** triplet excited state by MDEA is also thermodynamically favourable as $\Delta G_{\text{ET}}^{\text{EY-DA/MDEA}} = -0.31 \text{ eV} < 0$, considering the excited triplet state energy of **EY-DA**: $E_T^{\text{EY-DA}} = 1.88 \text{ eV}$ (extracted from **EY-DA** phosphorescence spectrum, **Error! Reference source not found.**). The rate constants for the reaction of triplet states of **EY-MA** with co-initiators were not accessible by laser flash photolysis because of the strong overlap of the radical ions with the triplet state of **EY-MA**⁶⁸.

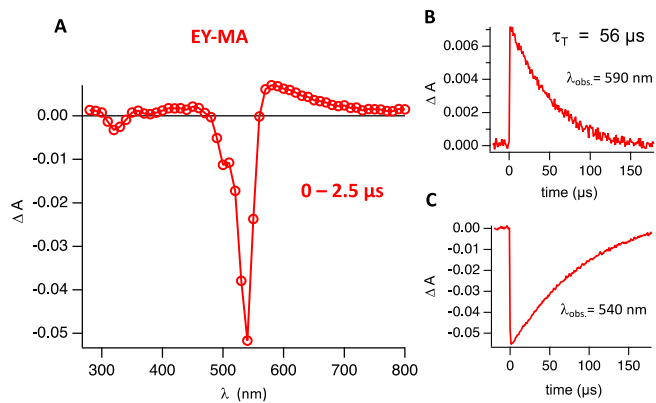


Figure 8. Transient absorption spectrum of a deoxygenated solution of **EY-MA** in ACN (A) from 0 to 2.5 μs after the laser pulse (532 nm, 7 ns pulse width). Decay traces at selected wavelengths (B and C).

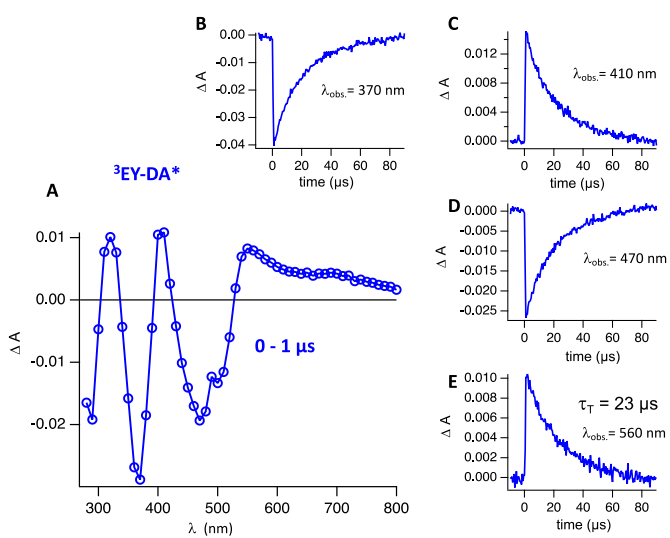


Figure 9. Transient absorption spectrum of a deoxygenated solution of **EY-DA** in ACN (A) from 0 to 1 μs after the laser pulse (355 nm, 7 ns pulse width). Decay traces at selected wavelengths (curves B to E).

Table 2. Photophysical parameters of the eosin Y derivatives.

	$\lambda_{\text{abs}}^{\text{max}}$ (nm) ^a	$\lambda_{\text{em}}^{\text{max}}$ (nm) ^a	$E_S^{\text{a,b}}$ (eV)	E_T^{c} (eV)	τ_S^{a} (ns)	τ_T^{a} (μs)	E_{ox}^{d} (V/SCE)	$E_{\text{red}}^{\text{d}}$ (V/SCE)
EY-MA	538	562	2.27	1.86	4.4	56	1.30 V	- 0.98 V
EY-DA	472	600	2.33	1.88	0.96	23	-	- 0.85 V

^a: in ACN, ^b: singlet state energy determined from fluorescence spectra (Figure 5), ^c: triplet state energy determined from phosphorescence spectra in ethanol glass at 77 K (**Error! Reference source not found.**), ^d: in DMF

Identification of radical species generated under irradiation: EPR experiments. EPR experiments were conducted to identify the radical species involved in the initiation of the photopolymerization reactions. The experiments were performed in dry THF for **EY-MA** and dry DCM for **EY-DA**, under argon atmosphere and using LED@405 nm as a visible light source.

In the absence of co-initiator, 120-s LED@405 nm irradiation of **EY-MA**/PBN in THF and **EY-DA**/PBN in DCM both led to the production of carbon-centred radicals as evidenced by the formation of characteristic PBN adducts ($a_N = 1.353$ mT, $a_H = 0.205$ mT, $g = 2.0064$ in THF and $a_N = 1.460$ mT, $a_H = 0.225$ mT, $g = 2.0059$ in DCM; **Error! Reference source not found.** and **Error! Reference source not found.**, adducts I), together with a nitroxide product derived from PBN ($a_N = 0.804$ mT, $g = 2.0069$ in THF and $a_N = 0.808$ mT, $g = 2.0065$ in DCM)⁶⁹.

After 120-s LED@405 nm irradiation, the **EY-MA**/PBN solution combined with MDEA in THF displayed an EPR signal with the following Hamiltonian parameters: $a_N = 1.480$ mT, $a_H = 0.233$ mT, $g = 2.0060$ (**Error! Reference source not found.**, adduct II). This signal is attributed to the spin trapping of aminoalkyl radicals by PBN (Figure 10-A) and was absent in the control without light. These observations support a single electron followed by a proton transfer reaction from MDEA to **EY-MA** under irradiation as previously described with EY⁵. Similar results were obtained following the 120-s LED@405 nm irradiation of **EY-DA**/MDEA/PBN in DCM (Figure 10-B) with the spin trapping of aminoalkyl radicals by PBN ($a_N = 1.496$ mT, $a_H = 0.347$ mT, $g = 2.0058$; **Error! Reference source not found.**, adduct II).

Figure 11 shows the experimental and simulated spectra of **EY-MA**/NAC/PBN and **EY-MA**/NAC/DMPO during *in situ* LED@405 nm irradiation. The characteristic 3-line signal of **EY-MA** semiquinone radical⁷⁰ dominates the spectra ($a_H(2H) = 0.347$ mT, $g = 2.0022$; **Error! Reference source not found.**, species A) and is superimposed with either the PBN- ($a_N = 1.417$ mT, $a_H = 0.250$ mT, $g =$

2.0067; **Error! Reference source not found.**, adduct III) or the DMPO-adduct of thiyl radical ($a_N = 1.366$ mT, $a_{H\beta} = 1.336$ mT, $a_{H\gamma} = 0.092$ mT, $a_{H\delta} = 0.065$ mT, $g = 2.0062$; **Error! Reference source not found.**, adduct IV). A similar amount of nitrene adducts is observed in the controls without light, suggesting also a nucleophilic addition of the thiol on the nitrene spin trap followed by oxidation (Forrester-Hepburn mechanism⁷¹).

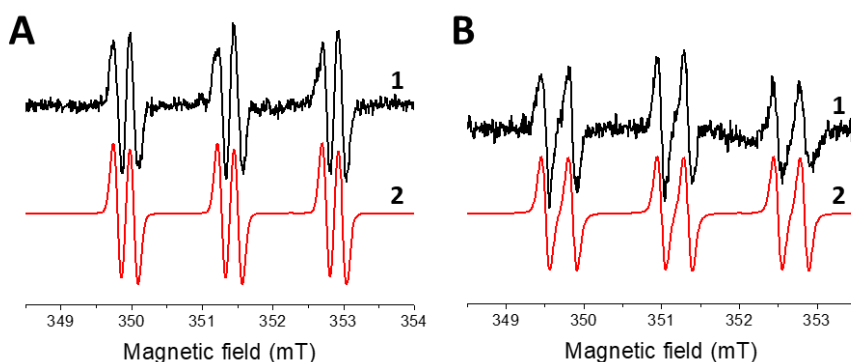


Figure 10. Experimental (1) and simulated (2) EPR spectra obtained after 120-s LED@405 nm irradiation of (A) **EY-MA**/MDEA/PBN in THF and (C) **EY-DA**/MDEA/PBN in DCM under argon, and (B) under *in situ* visible light irradiation of **EY-MA**/MDEA/DMPO in THF under argon.

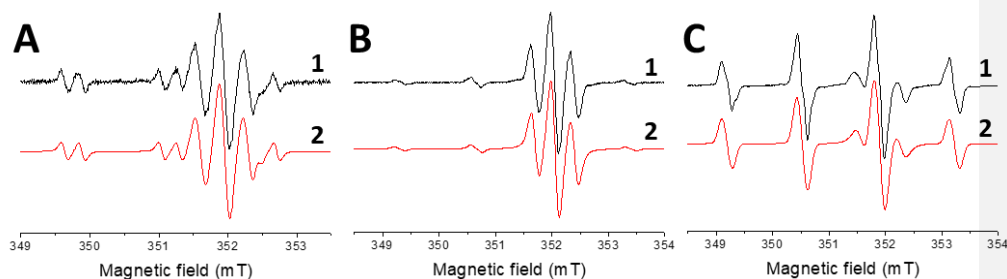


Figure 11. Experimental (1) and simulated (2) EPR spectra obtained under *in situ* visible light irradiation with a LED@405 nm of (A) **EY-MA**/NAC/PBN, (B) **EY-MA**/NAC/DMPO and (C) **EY-DA**/NAC/DMPO in THF under argon.

A mixture of **EY-DA**/Cys/DMPO in DCM was also analysed by EPR-ST under *in situ* LED@405 nm irradiation. The spectrum displayed in Figure 12-B is dominated by the triplet signal of **EY-DA** semiquinone radical ($a_{\text{H}(2\text{H})} = 0.329$ mT, $g = 2.0024$; **Error! Reference source not found.**, species A) overlapped with the signal of the DMPO-adduct of thiyl radical ($a_{\text{N}} = 1.382$ mT, $a_{\text{H}\beta} = 1.392$ mT, $a_{\text{H}\gamma} = 0.102$ mT, $a_{\text{H}\delta} = 0.079$ mT, $g = 2.0060$; **Error! Reference source not found.**, adduct V). The latter increased significantly compared to the control without light, supporting the formation of cysteamine-derived thiyl radicals upon irradiation of the **EY-DA**/Cys photoinitiating system. Similar results were obtained with **EY-MA**/Cys/DMPO solutions with the formation of a semiquinone radical ($a_{\text{H}(2\text{H})} = 0.319$ mT, $g = 2.0027$; **Error! Reference source not found.**, species A) and a mixture of Cys-DMPO adducts involving thiyl radicals (Figure 12-A).

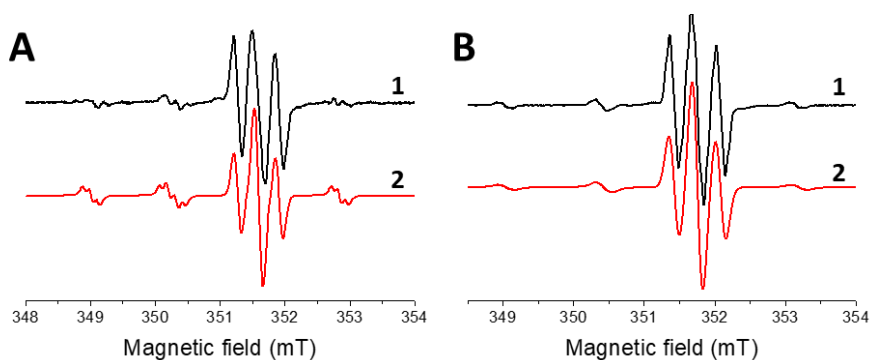


Figure 12. Experimental (1) and simulated (2) EPR spectra obtained under *in situ* LED@405 nm irradiation of (A) **EY-MA**/Cys/DMPO in THF and (B) **EY-DA**/Cys/DMPO in DCM, both of the solutions containing traces of MeOH, under argon.

Photopolymerization kinetic evaluations: radical photopolymerization kinetic study of a bio-based resin (SOA). The evaluation of the photopolymerization kinetics of the different eosin-based PIS was conducted with SOA, a promising bio-based acrylate monomer. PISs composed of MDEA, NAC or Cys were mixed with either EY, **EY-MA** or **EY-DA**, with [PS] = 0.5 wt% and [MDEA] = [NAC] = [Cys] = 2 wt% with respect to SOA (or TMPTA). The different systems were tested upon irradiation with the different visible light sources and compared with each other as well as with other common type II photoinitiators, *i.e.* non-functionalized eosin Y, camphorquinone (CQ)¹⁷ and benzophenone (BP)¹⁶. In a parallel attempt to increase the content of bio-based molecules, cysteamine (Cys) and N-acetyl-L-cysteine (NAC) were investigated as co-initiator alternatives as well. The kinetics of

photopolymerization of SOA were followed by real-time FTIR under irradiation with different visible LED sources. Since EY and **EY-MA** absorb up to 600 nm, the photopolymerization experiments were conducted with the following six LEDs operating 405 nm, 455 nm, 470nm, 505 nm,530 nm and 590 nm. Concerning **EY-DA**, LED@405 nm, LED@455 nm, LED@470 nm and LED@505 nm were employed since its absorbance spectrum is shifted towards the UV range. EY was used as a reference PS. SOA kinetic profiles are represented in Figure 13 and final acrylates conversions (FCs) obtained after 800 seconds of irradiation with **EY-MA** and **EY-DA** are summarized in Table 3 and compared with native EY, whose results are gathered in **Error! Reference source not found.** TMPTA kinetics are also shown in **Error! Reference source not found.** and the corresponding FCs obtained after 800 seconds of irradiation are gathered in **Error! Reference source not found.** for all the PISs examined.

Table 3. Final acrylate conversions of SOA (determined by FTIR) in the presence of PS/co-initiator where PS = **EY-MA** or **EY-DA** and co-initiator = MDEA, NAC or Cys in laminated conditions and under air after 800 s of irradiation with different LEDs. [**EY-MA**] = [**EY-DA**] = 0.5 wt%; [MDEA] = [NAC] = [Cys] = 2 wt%.

	405 nm	455 nm	470 nm	505 nm	530 nm	590 nm
EY-MA/MDEA/SOA	83% ^a , 56% ^b	77% ^a , 50% ^b	26% ^a , np ^b	65% ^a , 23% ^b	16% ^a , np ^b	21% ^a , np ^b
EY-MA/NAC/SOA	78% ^a , np ^b	51% ^a , np ^b	34% ^a , np ^b	33% ^a , np ^b	21% ^a , np ^b	10% ^a , np ^b
EY-MA/Cys/SOA	66% ^a , 41% ^b	25% ^a , 4% ^b	26% ^a , 9% ^b	25% ^a , 13% ^b	25% ^a , np ^b	np ^a , np ^b
EY-DA/MDEA/SOA	56% ^a , 35% ^b	44% ^a , 26% ^b	30% ^a , 17% ^b	18% ^a , np ^b	-	-
EY-DA/NAC/SOA	48% ^a , 26% ^b	48% ^a , 24% ^b	40% ^a , np ^b	34% ^a , np ^b	-	-
EY-DA/Cys/SOA	57% ^a , 21% ^b	35% ^a , 19% ^b	34% ^a , 16% ^b	37% ^a , np ^b	-	-

^a: in laminate, ^b: under air, np = no polymerization

Compared to TMPTA, the use of SOA in the PS/MDEA system led to much higher final conversions for a same set of conditions. In laminated conditions, FCs are higher than 65% and up to 83% were reached for the system based on **EY-MA** upon exposure to LED@405 nm, 455 nm and 505 nm. These results are particularly interesting as the conversions achieved with EY/MDEA remained lower upon the same time and light exposure. **EY-DA** exhibited good photo-initiating properties in laminate as well, reaching 56% of final acrylate conversion under irradiation with LED@405 nm. This is consistent with the efficient formation of MDEA-derived aminoalkyl radicals under irradiation, which was evidenced in the EPR-ST studies. Interestingly, the use of SOA increases final conversions reachable with the different systems under air since all the results obtained are higher than the ones observed when using

TMPTA with the same PISs. **EY-MA** even led to conversions higher than 50% upon exposure to LED@405 nm and 455 nm under air, which is remarkable considering that free radical photopolymerization is strongly inhibited by oxygen¹. This can be explained by the higher viscosity of SOA (15,000-38,000 cps) compared to TMPTA (106 cps), which prevents the renewing of oxygen within the sample during irradiation^{3,72}. Interestingly, when using tertiary amines as co-initiators, the reaction between the eosin derivatives and MDEA involves an electron transfer from the amine to their triplet excited states followed by a proton transfer under light exposure, leading thus to aminoalkyl radicals and eosin radical anions as described by EPR-ST results. The photoinduced electron transfer between **EY-MA** (acceptor) in its singlet state and MDEA (donor) is thermodynamically allowed according to the classical Rehm–Weller equation since $\Delta G_{\text{et}}^{\text{EY-MA/MDEA}} = -0.57$ eV. Reaction at the triplet state seems to be less favoured due to the high bimolecular quenching rate constant of **EY-MA** by oxygen ($k_q^{\text{O}_2} = 2.1 \times 10^9 \text{ M}^{-1} \cdot \text{s}^{-1}$). Under air, the aminoalkyl radicals which are considered as oxygen scavenger may react with oxygen to form peroxy radicals which could be involved in a H-abstraction reaction from the neighbouring amino groups, leading to the regeneration of the aminoalkyl radicals. Despite the high quenching rate constants of the triplet and singlet states of **EY-DA** with MDEA, *i.e.* $k_q^{\text{MDEA}}(^3\text{EY-DA}^*) = 1.5 \times 10^8 \text{ M}^{-1} \cdot \text{s}^{-1}$ and $k_q^{\text{MDEA}}(^1\text{EY-DA}^*) = 5.1 \times 10^9 \text{ M}^{-1} \cdot \text{s}^{-1}$, the reactivity of the **EY-DA**/MDEA-based PIS is lower than that observed with **EY-MA**/MDEA. This could be explained by the lower triplet and singlet lifetimes of **EY-DA** and the rapid photobleaching of the **EY-DA**/MDEA PIS at the ground state.

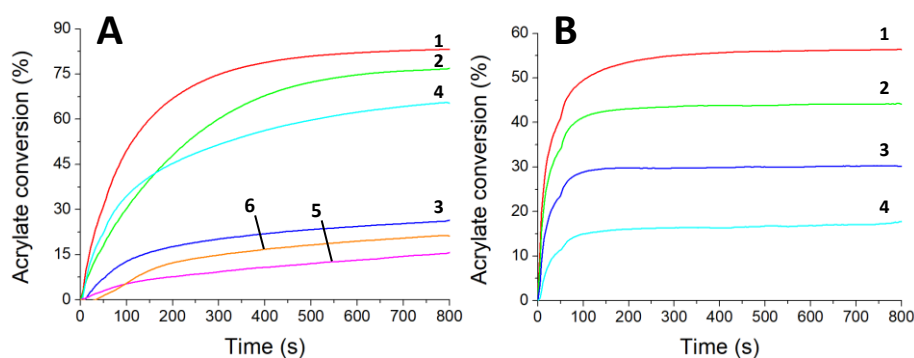


Figure 13. Kinetic profiles of SOA radical photopolymerization in the presence of (A) **EY-MA**/MDEA and (B) **EY-DA**/MDEA in laminated conditions under irradiation with (1) LED@405 nm, (2) LED@455 nm, (3) LED@470 nm, (4) LED@505 nm, (5) LED@530 nm and (6) LED@590 nm. $[\text{EY-MA}] = [\text{EY-DA}] = 0.5 \text{ wt\%}$, $[\text{MDEA}] = 2 \text{ wt\%}$.

Although MDEA proved to be an efficient co-initiator, *N*-acetyl-*L*-cysteine (NAC) and cysteamine (Cys) were studied as replacements in the aim to increase the bio-based content of the formulations. Considering their thiol function, NAC and Cys were all the more interesting as they could react with **EY-MA** and **EY-DA** to promote a thiol-acrylate reaction⁷³. PISs composed of PS/co-initiator, where co-initiator = NAC or Cys, were hence tested on the photopolymerization of SOA, under the same irradiation conditions as for the aforementioned studies ([PS] = 0.5 wt% and [NAC] = [Cys] = 2 wt% with respect to SOA). SOA photopolymerization kinetic profiles under different LED sources are presented in Figure 14 and in **Error! Reference source not found.**. FC results are summarized in Table 3 for **EY-MA** and **EY-DA**, and in **Error! Reference source not found.** for EY.

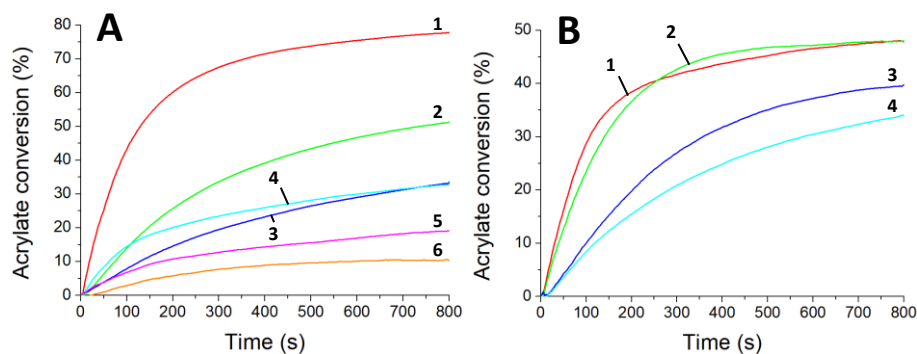


Figure 14. Kinetic profiles of SOA radical photopolymerization in the presence of (A) **EY-MA**/NAC and (B) **EY-DA**/NAC in laminated conditions under irradiation with (1) LED@405 nm, (2) LED@455 nm, (3) LED@470 nm, (4) LED@505 nm, (5) LED@530 nm and (6) LED@590 nm. [**EY-MA**] = [**EY-DA**] = 0.5 wt%, [NAC] = 2 wt%.

The thiol-acrylate polymerization initiated by the derivatives/NAC PISs successfully proceeded as thiol radicals were produced under light activation according to EPR-ST results. However, the efficiency of the addition of free radicals to acrylate functions controls the overall initiation efficiency of the polymerization process. As the sulphur-centred radicals are known to be less reactive towards double bonds³⁶ than carbon-centred radicals, it is not surprising that the initiating efficiency of eosin derivatives/NAC is lower than that when the derivatives are combined with MDEA in the same experimental conditions. FCs of 51% and 78% were still obtained with **EY-MA** upon exposure to LED@455 nm and LED@405 nm respectively, in laminated conditions, which is higher than the EY-

based system in the same conditions. For **EY-DA** combined with NAC, FCs were higher than 40% in laminate under LED@405 nm, 455 nm and 470 nm but rather low under air due to oxygen inhibition.

The kinetics experiments conducted on SOA using cysteamine as a co-initiator yielded satisfying results considering that FCs for both **EY-MA** and **EY-DA** were higher than those obtained using EY. When **EY-MA** was used as a PS in laminate, FCs reached 66% under LED@405 nm irradiation and averaged around 25% for the other light sources. Concerning **EY-DA**, 57% of acrylate conversation was obtained in laminate under LED@405 nm and conversions ranging from 34 to 37% were reached with the other LEDs, showing thus better photo-initiating properties than EY as well. The FCs of SOA are particularly low under air with both PISs, *i.e.* **EY-MA** (or **EY-DA**)/NAC, due to oxygen inhibition of the FRP.

Release experiments. In this work, eosin Y derivatives play several roles. In combination with an appropriate co-initiator and under the adequate light exposure, they allow for high acrylate conversions of SOA. This makes the synthesis of biosourced polymer coatings possible, in which the different PIs are incorporated. Moreover, given appropriate light exposition once more, the dyes in their excited states are able to react with surrounding oxygen to generate cytotoxic reactive oxygen species (ROS) locally, which confers antibacterial properties to the coatings in which they might be embedded. The main interest of eosin Y functionalization is to covalently graft the PS onto the polymer matrix as it forms, so it does not leach from it to the surrounding media during its application lifetime. If the dyes are indeed only encapsulated in the polymer matrix, they may undergo a progressive release out of the polymer network⁴⁵, causing the antibacterial effect to decrease over time. For a sustainable biocidal activity, it is then of the utmost importance that they remain bonded to the polymer coating. To study the release kinetics of the eosin Y derivatives, 1.5-cm pellets composed of AR87/MDEA/SOA, **EY-MA**/MDEA/SOA and **EY-DA**/MDEA/SOA were prepared in laminated conditions using LED@405 nm as a light source ([PS] = 0.5 wt% and [co-initiator] = 2 wt% according to SOA, **Error! Reference source not found.**). Tack-free materials were immersed in ACN and the PS mass loss from each pellet was kinetically evaluated using UV-visible spectroscopy. The results are reported in **Error! Reference source not found.** The functionalization of eosin Y and its copolymerization with SOA undeniably limits its release out of the polymer network. After 8 hours, the release percentage of AR87 was twice as high as the one of **EY-MA**, and at least 10 times higher than **EY-DA** release percentage. Although the release of **EY-MA** and **EY-DA** seemed to stabilize after 8 hours, AR87 release was still rising. The non-zero release values obtained for **EY-MA** and **EY-DA** must be caused by unreacted chemicals prone to migrate and thus leach out of the polymer network. **EY-MA** and **EY-DA** represent thus adequate

candidates for the synthesis of polymer coatings featuring potential sustainable antibacterial properties. However, considering synthesis yields and monomer FC rates, the evaluation of biocidal effect was conducted on **EY-MA**-based materials in the following sections.

Antibacterial properties assessment of the photoinduced materials. To evaluate **EY-MA** antibacterial performance, the first step is to investigate its ability to generate ROS and more particularly $^1\text{O}_2$ under visible light irradiation. DPBF is known to be a common trap for $^1\text{O}_2$ ⁷⁴. It reacts quickly with *in-situ* generated singlet oxygen to give 1,2-dibenzoylbenzene, a colourless product (**Error! Reference source not found.**)^{75,76}. This decomposition can be followed over time using UV-visible spectroscopy since DPBF features a maximal absorption band at 410 nm in methanol (Figure 15).

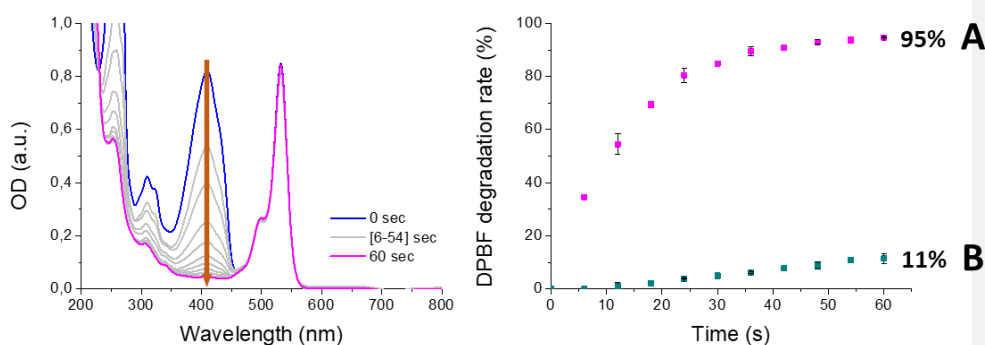


Figure 15. Evolution of DPBF absorption spectrum in presence of **EY-MA** in solution in MeOH under LED@530 nm irradiation (left). DPBF degradation rate (A) in presence of **EY-MA** and (B) alone under irradiation at LED@530 nm over time (right). [DPBF] = 1.48×10^{-5} M and [EY-MA] = 3.88×10^{-6} M.

The evolution of DPBF absorption spectrum was studied alone and in the presence of **EY-MA**. **EY-MA** remarkably accelerated DPBF photobleaching under irradiation. Its presence led to a 95% degradation rate of DPBF after a cumulative irradiation time of just one minute whereas DPBF decomposed to only 11% when irradiated alone. This indicates a high and quick production of $^1\text{O}_2$ by **EY-MA** upon visible light exposure. These results are highly encouraging for the *in vitro* assessment of antibacterial properties of the associated photo-induced materials against bacteria strains. The ability of **EY-MA**-derived polymer pellets to reduce bacterial surface adhesion was investigated against *S. aureus* and *E. coli*, with as well as without visible light activation. The samples were incubated either

in a *S. aureus* or in a *E. coli* suspension overnight to maximise bacterial adhesion. Half of the samples were then exposed to white visible light at 37 °C for 1 h on each side, while the other half of the pellets were stored in the dark at 37 °C. Figure 16 displays the number of CFU that grew overnight on the surface of the irradiated and non-irradiated pellets for both bacteria strains.

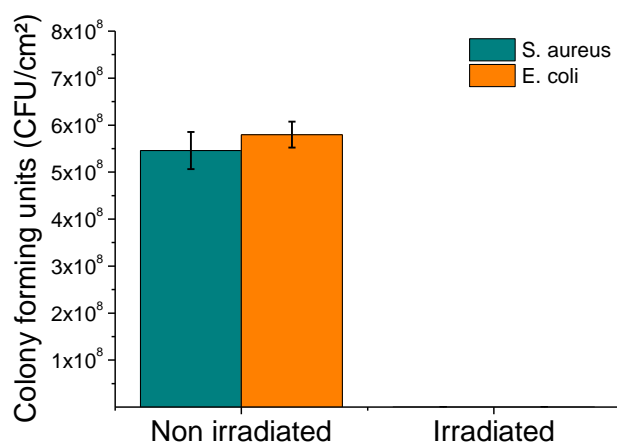


Figure 16. Antibacterial properties of the photoactive eosin Y-derived material against *E. coli* and *S. aureus*, with and without visible light exposure. Photoactive material = **EY-MA**/NAC/SOA (with 0.5 wt% of **EY-MA** and 2 wt% of NAC with respect to the monomer).

Figure 17 exhibits the petri dishes obtained for the solutions at 10^{-3} , 10^{-4} and 10^{-5} CFU/mL after 48 h of incubation at 37 °C, for *S. aureus* and *E. coli*, with and without visible light irradiation. Results evidence bacterial proliferation on non-irradiated pellets, which was to be expected since no antibacterial activity has been reported for soybean oil⁷⁷. On the other hand, almost complete bacterial inhibition was observed on their surface when the incubated materials were irradiated with visible light, regardless of the bacteria strain (Figure 16). The visible light exposure of the pellets allowed for more than 99.99% of inhibition for both *E. coli* and *S. aureus*. This result is likely due to the generation of 1O_2 on **EY-MA**-derived materials upon exposure to visible light as demonstrated above. This underlines the great potential of these materials to be used for antibacterial applications.

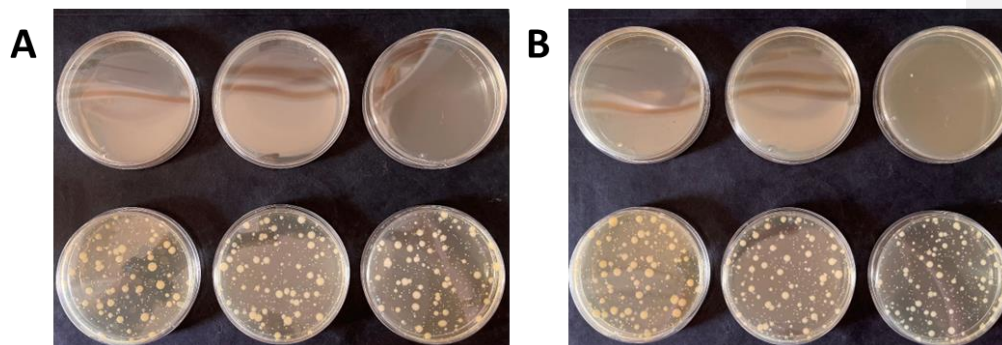


Figure 17. Antibacterial assay of the photoactive **EY-MA**-derived material against (A) *S. aureus* and (B) *E. coli*, with (top row) and without (bottom row) visible-light exposure. Concentrations were 10^{-3} (left), 10^{-4} (middle) and 10^{-5} CFU/mL (right) on each picture. Photoactive material = **EY-MA**/NAC/SOA (with 0.5 wt% of **EY-MA** and 2 wt% of NAC with respect to the monomer).

3D photo-printing studies. VAT photopolymerization printing technologies such as stereolithography or digital light processing (DLP) allows the production of customized objects with unique geometries and added value when active materials can be printed. The flexibility of these techniques enables the on-demand production of antibacterial objects and devices that can find application in several fields from biomedical to environmental science, as well as in a wide range of industrial sectors spanning from food and beverage to health risk mitigation. Preliminary photo-rheology tests were performed on two formulations composed of **EY-MA**/co-initiator/SOA (where co-initiator = MDEA or NAC) to investigate the suitability of the photosensitive formulations for DLP VAT photopolymerization and to obtain information to set the printing parameters (Figure 18).

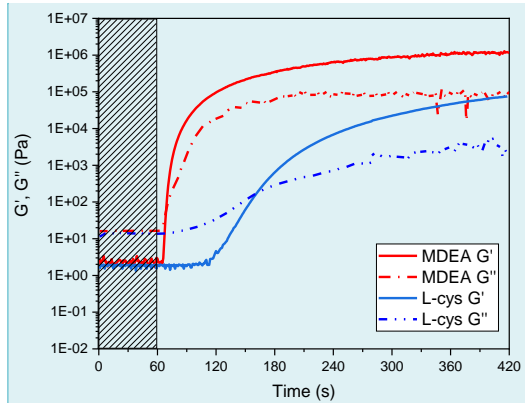


Figure 18. Photo-rheology tests performed on **EY-MA/MDEA/SOA** and **EY-MA/NAC/SOA** formulations ([**EY-MA**] = 0.5 wt%, [**MDEA**] = [**NAC**] = 2 wt%, LED @405 nm, light intensity 40 mW.cm⁻²). Light was turned on after 60 s.

When irradiated with a LED@405 nm, the formulation using MDEA as co-initiator is highly reactive as the gel point ($G' = G''$) is reached after only 10 seconds of irradiation concomitantly with a fast increase of the storage modulus (G'). On the contrary, the formulation containing NAC shows a lower reactivity than the MDEA-based one. The gel point is indeed reached after 100 s of irradiation with a lower polymerization rate (slope of the G' curve). This preliminary test showed the good suitability of the MDEA-based formulation for DLP printing with printing times similar to those of commercial formulations, while longer irradiation times are needed for the NAC-based formulation. Aiming to reduce the printing times, the polymerization vat was heated at 50°C and the layer thickness was set to 50 μm . The 3D printing of the **EY-MA/MDEA/SOA** formulation was easily done with relatively short printing times (8s/layer) giving thin-walled structures with good resolution and enabling the printing of multi-material devices presenting antibacterial channels. Despite the lower reactivity of the **EY-MA/NAC** photo-initiating system compared to the MDEA-based one, the **EY-MA/NAC/SOA** formulation has been successfully DLP printed with longer irradiation time (Figure 19).

Commented [LP1]: Je ne peux pas ouvrir ce fichier pour modifier la légende, un message d'erreur apparaît. Je n'ai pas non plus le fichier source

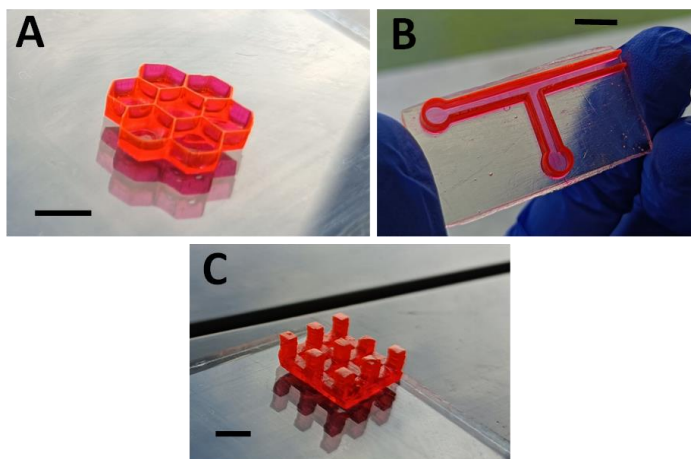


Figure 19. 3D-photoprinted materials by Digital Light Processing with (A and B) **EY-MA**/MDEA/SOA and (C) **EY-MA**/NAC/SOA under LED@405 nm irradiation ([**EY-MA**] = 0.5 wt%, [MDEA] = [NAC] = 2 wt%, irradiation intensity = 40 mW/cm²). Scale bars = 1 cm.

Conclusion

EY-MA and **EY-DA**, two copolymerizable derivatives of eosin Y, have been designed and synthesized to perform photopolymerization reactions of a bio-based acrylate monomer in the visible range. Both PS have demonstrated highly efficient photoinitiating properties for the free radical photopolymerization of SOA in combination with electron and/or H-donor co-initiators such as *N*-methyl-diethanolamine (MDEA), cysteamine (Cys) or *N*-acetyl-L-cysteine (NAC), and upon exposure to visible light sources (LED@405 and 455 nm). The acrylate FCs for SOA polymerization in the presence of **EY-MA**/MDEA-based PIS have reached for instance 83%, 77% and 65% with LEDs@405, 455 and 505 nm, respectively, and outperformed those obtained with EY and other common PS such as camphorquinone or BP. In an attempt to increase the use of bio-sourced compounds, we also demonstrated the efficient photoinitiating properties of systems based on **EY-MA** (or **EY-DA**)/NAC (or Cys) under LED@405 nm. These interesting results were supported by EPR-ST experiments which evidenced the formation of aminoalkyl and thiyl radicals responsible for the FRP and the thiol-acrylate polymerization processes. Also, the copolymerization of the functional EY-based PS within the polymer matrix has strongly limited their leakage out of the polymer network, allowing for the synthesis of photoactivable materials. The efficient singlet oxygen generation of the **EY-MA**-based materials has indeed led to tremendous antibacterial properties after visible light exposure, against both Gram-

positive *S. aureus* and Gram-negative *E. coli*. A 3-log adhesion decrease has been observed for *E. coli* and a 100% adhesion inhibition of *S. aureus* has been demonstrated after visible light exposure. Finally, complex 3D structures have been printed from SOA combined with PIS based on **EY-MA/MDEA or EY-MA/NAC** under with LED@405 nm irradiation. Consequently, the visible light-photosensitive and antibacterial formulations investigated in this study represent very interesting candidates for 3D-photoprinting applications combined with antibacterial purposes in mild conditions, such as the design of safe and biobased medical devices.

Author Contributions

The manuscript was written through the contributions of all authors. All authors have given approval to the final version of the manuscript.

Notes

The authors declare no competing financial interest.

Acknowledgments

Prof. Versace Davy-Louis would like to thank UPEC and the French National Agency for financial support (ANR project MIAM).

References

- (1) Yagci, Y.; Jockusch, S.; Turro, N. J. Photoinitiated Polymerization: Advances, Challenges, and Opportunities. *Macromolecules* **2010**, *43* (15), 6245–6260. <https://doi.org/10.1021/ma1007545>.
- (2) O'Brien, A. K.; Bowman, C. N. Impact of Oxygen on Photopolymerization Kinetics and Polymer Structure. *Macromolecules* **2006**, *39* (7), 2501–2506. <https://doi.org/10.1021/ma051863l>.
- (3) Tehfe, M.; Louradour, F.; Lalevée, J.; Fouassier, J.-P. Photopolymerization Reactions: On the Way to a Green and Sustainable Chemistry. *Applied Sciences* **2013**, *3* (2), 490–514. <https://doi.org/10.3390/app3020490>.
- (4) Topa-Skwarczyńska, M.; Ortyl, J. Photopolymerization Shrinkage: Strategies for Reduction, Measurement Methods and Future Insights. *Polym. Chem.* **2023**, *14* (18), 2145–2158. <https://doi.org/10.1039/D3PY00261F>.
- (5) Fouassier, J. P.; Lalevée, J. *Photoinitiators for Polymer Synthesis: Scope, Reactivity and Efficiency*; Wiley-VCH Verlag GmbH & Co. KGaA: Weinheim, Germany, 2012. <https://doi.org/10.1002/9783527648245>.

- (6) Xiao, P.; Zhang, J.; Dumur, F.; Tehfe, M. A.; Morlet-Savary, F.; Graff, B.; Gimes, D.; Fouassier, J. P.; Lalevéé, J. Visible Light Sensitive Photoinitiating Systems: Recent Progress in Cationic and Radical Photopolymerization Reactions under Soft Conditions. *Progress in Polymer Science* **2015**, *41*, 32–66. <https://doi.org/10.1016/j.progpolymsci.2014.09.001>.
- (7) Shao, J.; Huang, Y.; Fan, Q. Visible Light Initiating Systems for Photopolymerization: Status, Development and Challenges. *Polym. Chem.* **2014**, *5* (14), 4195–4210. <https://doi.org/10.1039/C4PY00072B>.
- (8) Garra, P.; Fouassier, J. P.; Lakhdar, S.; Yagci, Y.; Lalevéé, J. Visible Light Photoinitiating Systems by Charge Transfer Complexes: Photochemistry without Dyes. *Progress in Polymer Science* **2020**, *107*, 101277. <https://doi.org/10.1016/j.progpolymsci.2020.101277>.
- (9) Dumur, F. Recent Advances on Photobleachable Visible Light Photoinitiators of Polymerization. *Eur. Polym. J.* **2023**, *186*, 111874. <https://doi.org/10.1016/j.eurpolymj.2023.111874>.
- (10) El Hajj, Z.; Pierau, L.; Malval, J.-P.; Marrot, J.; Mazeran, P.-E.; Naoufal, D.; Ha-Thi, M.-H.; Steenkeste, K.; Dolbecq, A.; Floquet, S.; Oms, O.; Versace, D.-L.; Mialane, P. Shifting from UV to Visible-Light the Activity of Organic Photoinitiators via the Covalent Grafting of Polyoxometalates. *Macromolecules* **2023**, *56* (15), 6105–6116. <https://doi.org/10.1021/acs.macromol.3c00828>.
- (11) Elian, C.; Sanosa, N.; Bogliotti, N.; Herrero, C.; Sampedro, D.; Versace, D.-L. An Anthraquinone-Based Oxime Ester as a Visible-Light Photoinitiator for 3D Photoprinting Applications. *Polym. Chem.* **2023**, *14* (28), 3262–3269. <https://doi.org/10.1039/D3PY00681F>.
- (12) Breloy, L.; Brezová, V.; Richeter, S.; Clément, S.; Malval, J.-P.; Abbad Andaloussi, S.; Versace, D.-L. Bio-Based Porphyrins Pyropheophorbide *a* and Its Zn-Complex as Visible-Light Photosensitizers for Free-Radical Photopolymerization. *Polym. Chem.* **2022**, *13* (12), 1658–1671. <https://doi.org/10.1039/D1PY01714D>.
- (13) Breloy, L.; Brezová, V.; Barbieriková, Z.; Ito, Y.; Akimoto, J.; Chiappone, A.; Abbad-Andaloussi, S.; Malval, J.-P.; Versace, D.-L. Methacrylated Quinizarin Derivatives for Visible-Light Mediated Photopolymerization: Promising Applications in 3D-Printing Biosourced Materials under LED@405 Nm. *ACS Appl. Polym. Mater.* **2022**, *4* (1), 210–228. <https://doi.org/10.1021/acsapm.1c01210>.
- (14) Elian, C.; Brezová, V.; Sautrot-Ba, P.; Breza, M.; Versace, D.-L. Lawsone Derivatives as Efficient Photopolymerizable Initiators for Free-Radical, Cationic Photopolymerizations, and Thiol–Ene Reactions. *Polymers* **2021**, *13* (12), 2015. <https://doi.org/10.3390/polym13122015>.
- (15) Breloy, L.; Yavuz, O.; Yilmaz, I.; Yagci, Y.; Versace, D.-L. Design, Synthesis and Use of Phthalocyanines as a New Class of Visible-Light Photoinitiators for Free-Radical and Cationic Polymerizations. *Polym. Chem.* **2021**, *12* (30), 4291–4316. <https://doi.org/10.1039/D1PY00462J>.
- (16) Sautrot-Ba, P.; Brezová, V.; Malval, J.-P.; Chiappone, A.; Breloy, L.; Abbad-Andaloussi, S.; Versace, D.-L. Purpurin Derivatives as Visible-Light Photosensitizers for 3D Printing and Valuable Biological Applications. *Polym. Chem.* **2021**, *12* (17), 2627–2642. <https://doi.org/10.1039/D1PY00126D>.
- (17) Sautrot-Ba, P.; Jockusch, S.; Malval, J.-P.; Brezová, V.; Rivard, M.; Abbad-Andaloussi, S.; Blacha-Grzechnik, A.; Versace, D.-L. Quinizarin Derivatives as Photoinitiators for Free-Radical and Cationic Photopolymerizations in the Visible Spectral Range. *Macromolecules* **2020**, *53* (4), 1129–1141. <https://doi.org/10.1021/acs.macromol.9b02448>.
- (18) Breloy, L.; Brezová, V.; Blacha-Grzechnik, A.; Pisset, M.; Yildirim, M. S.; Yilmaz, I.; Yagci, Y.; Versace, D.-L. Visible Light Anthraquinone Functional Phthalocyanine Photoinitiator for Free-Radical and Cationic Polymerizations. *Macromolecules* **2020**, *53* (1), 112–124. <https://doi.org/10.1021/acs.macromol.9b01630>.
- (19) Breloy, L.; Losantos, R.; Sampedro, D.; Marazzi, M.; Malval, J.-P.; Heo, Y.; Akimoto, J.; Ito, Y.; Brezová, V.; Versace, D.-L. Allyl Amino-Thioxanthone Derivatives as Highly Efficient Visible Light H-Donors and Co-Polymerizable Photoinitiators. *Polym. Chem.* **2020**, *11* (26), 4297–4312. <https://doi.org/10.1039/D0PY00551G>.
- (20) Zhang, J.; Lalevéé, J.; Zhao, J.; Graff, B.; Stenzel, M. H.; Xiao, P. Dihydroxyanthraquinone Derivatives: Natural Dyes as Blue-Light-Sensitive Versatile Photoinitiators of

- Photopolymerization. *Polym. Chem.* **2016**, *7* (47), 7316–7324. <https://doi.org/10.1039/C6PY01550F>.
- (21) Kutahya, C.; Aykac, F. S.; Yilmaz, G.; Yagci, Y. LED and Visible Light-Induced Metal Free ATRP Using Reducible Dyes in the Presence of Amines. *Polym. Chem.* **2016**, *7* (39), 6094–6098. <https://doi.org/10.1039/C6PY01417H>.
- (22) Abdallah, M.; Dumur, F.; Graff, B.; Hijazi, A.; Lalevée, J. High Performance Dyes Based on Triphenylamine, Cinnamaldehyde and Indane-1,3-Dione Derivatives for Blue Light Induced Polymerization for 3D Printing and Photocomposites. *Dyes and Pigments* **2020**, *182*, 108580. <https://doi.org/10.1016/j.dyepig.2020.108580>.
- (23) Abdallah, M.; Hijazi, A.; Graff, B.; Fouassier, J.-P.; Rodeghiero, G.; Gualandi, A.; Dumur, F.; Cozzi, P. G.; Lalevée, J. Coumarin Derivatives as Versatile Photoinitiators for 3D Printing, Polymerization in Water and Photocomposite Synthesis. *Polym. Chem.* **2019**, *10* (7), 872–884. <https://doi.org/10.1039/C8PY01708E>.
- (24) Waite, J. G.; Yousef, A. E. Chapter 3 Antimicrobial Properties of Hydroxyxanthenes. In *Advances in Applied Microbiology*; Elsevier, 2009; Vol. 69, pp 79–98. [https://doi.org/10.1016/S0065-2164\(09\)69003-1](https://doi.org/10.1016/S0065-2164(09)69003-1).
- (25) Chibac, A. L.; Melinte, V.; Brezová, V.; Renard, E.; Brosseau, A.; Langlois, V.; Versace, D. Metal-Free and Heterogeneous Photocatalytic Reduction of 4-Nitroaniline by a Poly(Ethylene Glycol)-Supported Eosin Dye under Visible-Light Exposure. *ChemCatChem* **2019**, *11* (14), 3307–3317. <https://doi.org/10.1002/cctc.201900040>.
- (26) Derayea, S. M.; Nagy, D. M. Application of a Xanthene Dye, Eosin Y, as Spectroscopic Probe in Chemical and Pharmaceutical Analysis; a Review. *Rev. Anal. Chem.* **2018**, *37* (3). <https://doi.org/10.1515/revac-2017-0020>.
- (27) Alturkistani, H. A.; Tashkandi, F. M.; Mohammedsleh, Z. M. Histological Stains: A Literature Review and Case Study. *Glob. J. Health Sci.* **2016**, *8* (3), 72–79. <https://doi.org/10.5539/gjhs.v8n3p72>.
- (28) Diercxsens, N. Eosin Y. In *Encyclopedia of Reagents for Organic Synthesis (EROS)*; John Wiley & Sons, Ltd, 2017; pp 1–3. <https://doi.org/10.1002/047084289X.rn02033>.
- (29) Bosveli, A.; Montagnon, T.; Kalaitzakis, D.; Vassilikogiannakis, G. Eosin: A Versatile Organic Dye Whose Synthetic Uses Keep Expanding. *Org. Biomol. Chem.* **2021**, *19* (15), 3303–3317. <https://doi.org/10.1039/D1OB00301A>.
- (30) Kuck, L. R.; Taylor, A. W. Photopolymerization as an Innovative Detection Technique for Low-Density Microarrays. *BioTechniques* **2008**, *45* (2), 179–186. <https://doi.org/10.2144/000112889>.
- (31) Avens, H. J.; Bowman, C. N. Mechanism of Cyclic Dye Regeneration during Eosin-sensitized Photoinitiation in the Presence of Polymerization Inhibitors. *J. Polym. Sci. A Polym. Chem.* **2009**, *47* (22), 6083–6094. <https://doi.org/10.1002/pola.23649>.
- (32) Fouassier, J. P.; Chesneau, E. Polymérisation Induite Sous Irradiation Laser Visible, 4. Le Système Éosine/Photoamorceur Ultra-violet/Amine. *Makromol. Chem.* **1991**, *192* (2), 245–260. <https://doi.org/10.1002/macp.1991.021920206>.
- (33) Kumar, G. S.; Neckers, D. C. Laser-Induced Three-Dimensional Photopolymerization Using Visible Initiators and UV Cross-Linking by Photosensitive Comonomers. *Macromolecules* **1991**, *24* (15), 4322–4327. <https://doi.org/10.1021/ma00015a013>.
- (34) Mallavia, R.; Amat-Guerri, F.; Fimia, A.; Sastre, R. Synthesis and Evaluation as a Visible-Light Polymerization Photoinitiator of a New Eosin Ester with an O-Benzoyl- α -Oxoxime Group. *Macromolecules* **1994**, *27* (9), 2643–2646. <https://doi.org/10.1021/ma00087a041>.
- (35) Burget, D.; Fouassier, J. P.; Amat-Guerri, F.; Mallavia, R.; Sastre, R. Enhanced Activity as Polymerization Photoinitiators of Rose Bengal and Eosin Esters with an O-Benzoyl- α -Oxoxime Group: The Role of the Excited State Reactivity. *Acta Polym.* **1999**, *50* (9), 337–346. [https://doi.org/10.1002/\(SICI\)1521-4044\(19990901\)50:9<337::AID-APOL337>3.0.CO;2-I](https://doi.org/10.1002/(SICI)1521-4044(19990901)50:9<337::AID-APOL337>3.0.CO;2-I).
- (36) Popielarz, R.; Vogt, O. Effect of Coinitiator Type on Initiation Efficiency of Two-component Photoinitiator Systems Based on Eosin. *J. Polym. Sci. A Polym. Chem.* **2008**, *46* (11), 3519–3532. <https://doi.org/10.1002/pola.22688>.

- (37) Neumann, M. G.; Schmitt, C. C.; Maciel, H. The Photopolymerization of Styrenesulfonate Initiated by Dyes. *J. Photochem. Photobiol. A* **2005**, *175* (1), 15–21. <https://doi.org/10.1016/j.jphotochem.2005.03.024>.
- (38) Avens, H. J.; Randle, T. J.; Bowman, C. N. Polymerization Behavior and Polymer Properties of Eosin-Mediated Surface Modification Reactions. *Polymer* **2008**, *49* (22), 4762–4768. <https://doi.org/10.1016/j.polymer.2008.08.054>.
- (39) Encinas, M. V.; Rufs, A. M.; Bertolotti, S. G.; Previtali, C. M. Xanthene Dyes/Amine as Photoinitiators of Radical Polymerization: A Comparative and Photochemical Study in Aqueous Medium. *Polymer* **2009**, *50* (13), 2762–2767. <https://doi.org/10.1016/j.polymer.2009.04.024>.
- (40) Sharifi, S.; Sharifi, H.; Akbari, A.; Chodosh, J. Systematic Optimization of Visible Light-Induced Crosslinking Conditions of Gelatin Methacryloyl (GelMA). *Sci. Rep.* **2021**, *11* (1), 23276. <https://doi.org/10.1038/s41598-021-02830-x>.
- (41) Hao, Y.; Shih, H.; Muñoz, Z.; Kemp, A.; Lin, C.-C. Visible Light Cured Thiol-Vinyl Hydrogels with Tunable Degradation for 3D Cell Culture. *Acta Biomater.* **2014**, *10* (1), 104–114. <https://doi.org/10.1016/j.actbio.2013.08.044>.
- (42) González-Vidal, N.; Martínez De Ilarduya, A.; Muñoz-Guerra, S. Poly(Ethylene-Co-1,4-cyclohexylenedimethylene Terephthalate) Copolyesters Obtained by Ring Opening Polymerization. *J. Polym. Sci. A Polym. Chem.* **2009**, *47* (22), 5954–5966. <https://doi.org/10.1002/pola.23639>.
- (43) Bahney, C. S.; Lujan, T. J.; Hsu, C. W.; Bottlang, M.; West, J. L.; Johnstone, B. Visible Light Photoinitiation of Mesenchymal Stem Cell-Laden Bioresponsive Hydrogels. *Eur. Cells Mater.* **2011**, *22*, 43–55.
- (44) Zhang, M.-D.; Huang, X.; Li, Z.; Song, W.; Kong, Y.; Zhang, C.; Liang, L.-T.; Huang, Y.-Y.; Tan, Y.-X.; Feng, Y.; Liu, Q.-H.; Zhao, Y.-X.; Fu, X.-B.; Huang, S. White-Light-Induced Synthesis of Injectable Alginate-Based Composite Hydrogels for Rapid Hemostasis. *Mil. Med. Res.* **2023**, *10* (1), 47. <https://doi.org/10.1186/s40779-023-00483-7>.
- (45) Sautrot-Ba, P.; Contreras, A.; Abbad Andaloussi, S.; Coradin, T.; Hélar, C.; Razza, N.; Sangermano, M.; Mazeran, P.-E.; Malval, J.-P.; Versace, D.-L. Eosin-Mediated Synthesis of Polymer Coatings Combining Photodynamic Inactivation and Antimicrobial Properties. *J. Mater. Chem. B* **2017**, *5* (36), 7572–7582. <https://doi.org/10.1039/C7TB01358B>.
- (46) Santos, A. R.; Da Silva, A. F.; Batista, A. F. P.; Freitas, C. F.; Bona, E.; Sereia, M. J.; Caetano, W.; Hioka, N.; Mikcha, J. M. G. Application of Response Surface Methodology to Evaluate Photodynamic Inactivation Mediated by Eosin Y and 530 Nm LED against Staphylococcus Aureus. *Antibiotics* **2020**, *9* (3), 125. <https://doi.org/10.3390/antibiotics9030125>.
- (47) Andrzej, J.; Stanislaw, J.; Agnieszka, M.; Joanna, N. The Action of Photosensitizers and Serum in a Bactericidal Process. II. The Effects of Dyes: Hypericin, Eosin Y and Saphranin O. *Polish Journal of Microbiology* **2005**, *54* (4), 323–330.
- (48) Bonin, E.; Dos Santos, A. R.; Fiori Da Silva, A.; Ribeiro, L. H.; Favero, M. E.; Campanerut-Sá, P. A. Z.; De Freitas, C. F.; Caetano, W.; Hioka, N.; Mikcha, J. M. G. Photodynamic Inactivation of Foodborne Bacteria by Eosin Y. *J. Appl. Microbiol.* **2018**, *124* (6), 1617–1628. <https://doi.org/10.1111/jam.13727>.
- (49) Marinic, K.; Manoil, D.; Filieri, A.; Wataha, J. C.; Schrenzel, J.; Lange, N.; Bouillaguet, S. Repeated Exposures to Blue Light-Activated Eosin Y Enhance Inactivation of E. Faecalis Biofilms, in Vitro. *Photodiagnosis Photodyn. Ther.* **2015**, *12* (3), 393–400. <https://doi.org/10.1016/j.pdpdt.2015.06.004>.
- (50) Staneva, D.; Yordanova, S.; Vasileva-Tonkova, E.; Stoyanov, S.; Grabchev, I. Photophysical and Antibacterial Activity of Light-Activated Quaternary Eosin Y. *Open Chem.* **2019**, *17* (1), 1244–1251. <https://doi.org/10.1515/chem-2019-0135>.
- (51) Romano, I.; Ayadi, F.; Rizzello, L.; Summa, M.; Bertorelli, R.; Pompa, P. P.; Brandi, F.; Bayer, I. S.; Athanassiou, A. Controlled Antiseptic/Eosin Release from Chitosan-Based Hydrogel Modified Fibrous Substrates. *Carbohydr. Polym.* **2015**, *131*, 306–314. <https://doi.org/10.1016/j.carbpol.2015.05.057>.

- (52) Johnson, G. A.; Muthukrishnan, N.; Pellois, J.-P. Photoinactivation of Gram Positive and Gram Negative Bacteria with the Antimicrobial Peptide (KLAKLAK)₂ Conjugated to the Hydrophilic Photosensitizer Eosin Y. *Bioconjugate Chem.* **2013**, *24* (1), 114–123. <https://doi.org/10.1021/bc3005254>.
- (53) Zhu, Y.; Xu, C.; Zhang, N.; Ding, X.; Yu, B.; Xu, F.-J. Polycationic Synergistic Antibacterial Agents with Multiple Functional Components for Efficient Anti-Infective Therapy. *Adv. Funct. Mater.* **2018**, *28* (14), 1706709. <https://doi.org/10.1002/adfm.201706709>.
- (54) Stoll, S.; Schweiger, A. EasySpin, a Comprehensive Software Package for Spectral Simulation and Analysis in EPR. *J. Magn. Reson.* **2006**, *178* (1), 42–55. <https://doi.org/10.1016/j.jmr.2005.08.013>.
- (55) Suppan, P.; Vauthey, E. The Energy Balance of Photoinduced Electron Transfer Reactions. *Journal of Photochemistry and Photobiology A: Chemistry* **1989**, *49* (1–2), 239–248. [https://doi.org/10.1016/1010-6030\(89\)87121-7](https://doi.org/10.1016/1010-6030(89)87121-7).
- (56) Yagci, Y.; Jockusch, S.; Turro, N. J. Mechanism of Photoinduced Step Polymerization of Thiophene by Onium Salts: Reactions of Phenyliodonium and Diphenylsulfonium Radical Cations with Thiophene. *Macromolecules* **2007**, *40* (13), 4481–4485. <https://doi.org/10.1021/ma070586a>.
- (57) Esumi, N.; Suzuki, K.; Nishimoto, Y.; Yasuda, M. Synthesis of 1,4-Dicarbonyl Compounds from Silyl Enol Ethers and Bromocarbonyls, Catalyzed by an Organic Dye under Visible-Light Irradiation with Perfect Selectivity for the Halide Moiety over the Carbonyl Group. *Org. Lett.* **2016**, *18* (21), 5704–5707. <https://doi.org/10.1021/acs.orglett.6b02869>.
- (58) Pellosi, D. S.; Estevão, B. M.; Freitas, C. F.; Tsubone, T. M.; Caetano, W.; Hioka, N. Photophysical Properties of Erythrosin Ester Derivatives in Ionic and Non-Ionic Micelles. *Dyes Pigm.* **2013**, *99* (3), 705–712. <https://doi.org/10.1016/j.dyepig.2013.06.026>.
- (59) Nan, X.; Huang, Y.; Fan, Q.; Shao, J. Efficient Visible Photoinitiator Containing Linked Dye-Coinitiator and Iodonium Salt for Free Radical Polymerization. *Prog. Org. Coat.* **2015**, *81*, 11–18. <https://doi.org/10.1016/j.porgcoat.2014.12.013>.
- (60) Amat-Guerri, F.; López-González, M. M. C.; Martínez-Utrilla, R.; Sastre, R. Synthesis and Spectroscopic Properties of New Rose Bengal and Eosin Y Derivatives. *Dyes Pigm.* **1990**, *12* (4), 249–272. [https://doi.org/10.1016/0143-7208\(90\)85017-l](https://doi.org/10.1016/0143-7208(90)85017-l).
- (61) Neckers, D. C.; Valdes-Aguilera, O. M. Photochemistry of the Xanthene Dyes. In *Advances in Photochemistry*; Volman, D. H., Hammond, G. S., Neckers, D. C., Eds.; John Wiley & Sons, Inc.: Hoboken, NJ, USA, 2007; pp 315–394. <https://doi.org/10.1002/9780470133491.ch4>.
- (62) Sandholzer, M.; Schuster, M.; Varga, F.; Liska, R.; Slugovc, C. ROMP Based Photoinitiator-Coinitiator Systems with Improved Migration Stability. *J. Polym. Sci. A Polym. Chem.* **2008**, *46* (11), 3648–3661. <https://doi.org/10.1002/pola.22705>.
- (63) Estevão, B. M.; Pellosi, D. S.; de Freitas, C. F.; Vanzin, D.; Franciscato, D. S.; Caetano, W.; Hioka, N. Interaction of Eosin and Its Ester Derivatives with Aqueous Biomimetic Micelles: Evaluation of Photodynamic Potentialities. *J. Photochem. Photobiol. A* **2014**, *287*, 30–39. <https://doi.org/10.1016/j.jphotochem.2014.04.015>.
- (64) Konstantinova, T. N.; Bojinov, V. B. Synthesis of Some Unsaturated 9-Phenylxanthene Dyes. *Dyes Pigm.* **1998**, *39* (2), 69–75. [https://doi.org/10.1016/S0143-7208\(97\)00071-5](https://doi.org/10.1016/S0143-7208(97)00071-5).
- (65) Amat-Guerri, F.; López-González, M. M. C.; Martínez-Utrilla, R.; Sastre, R. Singlet Oxygen Photogeneration by Ionized and Un-Ionized Derivatives of Rose Bengal and Eosin Y in Diluted Solutions. *Journal of Photochemistry and Photobiology A: Chemistry* **1990**, *53* (2), 199–210. [https://doi.org/10.1016/1010-6030\(90\)87124-T](https://doi.org/10.1016/1010-6030(90)87124-T).
- (66) Del Valle, J. C.; Catalán, J.; Amat-Guerri, F. Comparative Photophysical Study of Rose Bengal, Eosin Y and Their Monomethyl and Dimethyl Derivatives. *J. Photochem. Photobiol. A* **1993**, *72* (1), 49–53. [https://doi.org/10.1016/1010-6030\(93\)85084-L](https://doi.org/10.1016/1010-6030(93)85084-L).
- (67) Kim, D.; Stansbury, J. W. A Photo-Oxidizable Kinetic Pathway of Three-Component Photoinitiator Systems Containing Porphyrin Dye (Zn-Tpp), an Electron Donor and Diphenyl Iodonium Salt. *J. Polym. Sci. A Polym. Chem.* **2009**, *47* (12), 3131–3141. <https://doi.org/10.1002/pola.23401>.

- (68) Görner, H. Oxygen Uptake Induced by Electron Transfer from Donors to the Triplet State of Methylene Blue and Xanthene Dyes in Air-Saturated Aqueous Solution. *Photochem. Photobiol. Sci.* **2008**, *7* (3), 371–376. <https://doi.org/10.1039/b712496a>.
- (69) Ebersson, L. 'Inverted Spin Trapping'. Reactions between the Radical Cation of α -Phenyl-N-Tert-Butylnitrone and Ionic and Neutral Nucleophiles. *J. Chem. Soc., Perkin Trans. 2* **1992**, *0* (10), 1807–1813. <https://doi.org/10.1039/P29920001807>.
- (70) Brezová, V.; Pigošová, J.; Havlínová, B.; Dvoranová, D.; Ďurovič, M. EPR Study of Photochemical Transformations of Triarylmethane Dyes. *Dyes Pigm.* **2004**, *61* (2), 177–198. <https://doi.org/10.1016/j.dyepig.2003.10.012>.
- (71) Potapenko, D. I.; Bagryanskaya, E. G.; Tsentelovich, Y. P.; Reznikov, V. A.; Clanton, T. L.; Khrantsov, V. V. Reversible Reactions of Thiols and Thiyl Radicals with Nitron Spin Traps. *J. Phys. Chem. B* **2004**, *108* (26), 9315–9324. <https://doi.org/10.1021/jp049026t>.
- (72) Lai, H.; Peng, X.; Li, L.; Zhu, D.; Xiao, P. Novel Monomers for Photopolymer Networks. *Prog. Polym. Sci.* **2022**, *128*, 101529. <https://doi.org/10.1016/j.progpolymsci.2022.101529>.
- (73) Hoyle, C. E.; Bowman, C. N. Thiol–Ene Click Chemistry. *Angewandte Chemie International Edition* **2010**, *49* (9), 1540–1573. <https://doi.org/10.1002/anie.200903924>.
- (74) Wu, H.; Song, Q.; Ran, G.; Lu, X.; Xu, B. Recent Developments in the Detection of Singlet Oxygen with Molecular Spectroscopic Methods. *TrAC Trends in Analytical Chemistry* **2011**, *30* (1), 133–141. <https://doi.org/10.1016/j.trac.2010.08.009>.
- (75) Gollnick, K.; Schenck, G. O. Oxygen as a Dienophile. In *Organic Chemistry*; Elsevier, 1967; Vol. 8, pp 255–344. <https://doi.org/10.1016/B978-0-12-395743-6.50015-6>.
- (76) Carloni, P.; Damiani, E.; Greci, L.; Stipa, P.; Tanfani, F.; Tartaglini, E.; Wozniak, M. On the Use of 1,3-Diphenylisobenzofuran (DPBF). Reactions with Carbon and Oxygen Centered Radicals in Model and Natural Systems. *Res. Chem. Intermed.* **1993**, *19* (5), 395–405. <https://doi.org/10.1163/156856793X00181>.
- (77) P. Silva, L.; A. Joanitti, G.; Roberto S. A. Leite, J.; B. Azevedo, R. Comparative Study of the Antimicrobial Activities and Mammalian Cytotoxicity of 10 Fatty Acid-Rich Oils and Fats from Animal and Vegetable. *Nat. Prod. J.* **2011**, *1* (1), 40–46. <https://doi.org/10.2174/2210315511101010040>.

